A theoretical study of surfactant and liquid delivery into the lung

D. HALPERN,[1] O. E. JENSEN,[2] AND J. B. GROTBERG[3]
[1]*Department of Mathematics, University of Alabama, Tuscaloosa, Alabama 35487;*
[2]*Department of Applied Mathematics and Theoretical Physics, University of Cambridge, Cambridge CB3 9EW, United Kingdom; and* [3]*Department of Biomedical Engineering, Northwestern University, Evanston, 60208, and Department of Anesthesiology, Northwestern University Medical School, Chicago, Illinois 60611*

Halpern, D., O. E. Jensen, and J. B. Grotberg. A theoretical study of surfactant and liquid delivery into the lung. *J. Appl. Physiol.* 85(1): 333–352, 1998.—A computational study is presented for the transport of liquids and insoluble surfactant through the lung airways, delivered from a source at the distal end of the trachea. Four distinct transport regimes are considered: *1*) the instilled bolus may create a liquid plug that occludes the large airways but is forced peripherally during mechanical ventilation; *2*) the bolus creates a deposited film on the airway walls, either from the liquid plug transport or from direct coating, that drains under the influence of gravity through the first few airway generations; *3*) in smaller airways, surfactant species form a surface layer that spreads due to surface-tension gradients, i.e., Marangoni flows; and *4*) the surfactant finally reaches the alveolar compartment where it is cleared according to first-order kinetics. The time required for a quasi-steady-state transport process to evolve and for the subsequent delivery of the dose is predicted. Following fairly rapid transients, on the order of seconds, steady-state transport develops and is governed by the interaction of Marangoni flow and alveolar kinetics. Total delivery time is ~24 h for a typical first dose. Numerical solutions show that both transit and delivery times are strongly influenced by the strength of the preexisting surfactant and the geometric properties of the airway network. Delivery times for follow-up doses can increase significantly as the level of preexisting surfactant rises.

pulmonary surfactant; drug delivery; surfactant replacement therapy; respiratory distress syndrome; Marangoni flow; airway liquid; surface tension dynamics; pulmonary fluid mechanics

DIRECT INSTILLATION of a liquid bolus into the lung is common to a number of pulmonary events and clinical treatments. For example, partial liquid ventilation, when using perfluorocarbon liquids, has been suggested for treating respiratory distress syndrome (RDS) either in place of, or in conjunction with, surfactant-replacement therapy (SRT) (20, 50, 72, 79). Perfluorocarbon liquids have low surface tension and high oxygen and carbon dioxide solubilities and have been shown to improve lung mechanics and gas exchange. As another example, present investigations of gene therapy for cystic fibrosis and α-1 antitrypsin deficiency utilize delivery of the vector (e.g., adenovirus, liposome) onto the airway epithelial cells by liquid bolus (4, 8, 10, 37). Liquid delivery has also been recognized as a potential means to "piggyback" delivery of drugs (e.g., during cardiopulmonary resuscitation) and unwanted environmental toxins (22, 44, 49). Introduction of liquids into the lung also occurs in therapeutic and diagnostic bronchial alveolar lavage. A very prevalent application is SRT.

The delivery of exogenous surfactants into the lung for SRT is now a standard treatment for neonates with RDS (9, 46, 48, 54). In some studies, it has reduced infant mortality by one-half (54). The delivery method may be a bolus instilled into the trachea or an aerosol mixture (51, 81) and has been studied either as a prophylactic dose at birth or as rescue doses given several hours after delivery (48). At this juncture, the more popular treatment is the intratracheal bolus that spreads by a combination of various physical forces. The initial spreading can be quite rapid (11), reaching substantial amounts of the lung fields in 20 s. The early response of improved oxygenation for the patient appears to be due to an increase in functional residual capacity (25). Exogenous surfactant administration has also been used as a therapy for acute RDS (ARDS) (53, 69), for sepsis-induced ARDS (3) by aerosol, for mitigation of oxygen-toxic lung injury (56) and wood-smoke inhalation injury (18), for improvement of lung transplant results (58), and for treatment of meconium aspiration (78).

Strategies for optimizing liquid delivery into the lung depend, necessarily, on the particular application (SRT, liquid ventilation, gene therapy, drug delivery, etc.). In some cases, it may be desirable to transport the liquid primarily to the alveoli, in others, it may be more effective to coat primarily the airways. It may be important for the liquid to spread homogeneously or to be directed preferentially to specific lobes or generations. The residence time could be long or short. It may be advantageous to "blow" the liquid as a plug into the airways or to let it drain slowly into the lung.

In SRT, several parameters involving the physiology and the delivery technique may affect the transport

(67): the bolus volume (24); its injection rate (73); gravity and orientation (73); development of airway occlusion by the liquid; ventilation parameters at normal or high frequency (38, 65); the viscosity and surface tension of the fluid injected; the dose strength; the instillation site; and repeat-dosing protocols and intervals. There is evidence, for example, that a second dose of SRT tends to distribute to lung regions where the first dose was transported (73), possibly because of the opening of airways and ease of transport for the second dose through them. On the other hand, there may be delays in second-dose transport because the first dose ultimately lowers the surface-tension gradient driving the flow of the second dose (28). It is known, for example, that the second and following doses can be much less effective than the first dose (54), possibly because of the reduced gradient. The clearance of instilled surfactants is also very important in the overall transport, as is discussed below. In clinical studies, the nonresponse rate to instilled surfactants ranges from 15 to 35%, for example, depending on the study and patient group. Could the lack of response be due, in part, to inadequate surfactant transport and delivery? Consider the delivery pathway of a liquid bolus as it makes its way from the trachea to the alveoli. It may start as a liquid plug, progress to a deposited film lining the airways, establish a surface layer, and then reach the alveolar compartment. These four transport regimes are dominated by different physical forces.

The liquid-plug transport regime occurs if the liquid volume instilled is large enough and given over a short enough period for it to occlude the airway. Then the plug flow is driven by the pressure drop across the plug during inspiration, and the resulting motion depends on its viscosity, density, surface tension, and gravity. As the plug is blown peripherally, it deposits its liquid onto the airway wall, leaving behind a trailing film the thickness of which depends on the system parameters. Eventually, through the action of subdividing at airway bifurcations and depositing its mass onto the airway wall, the plug will lose enough liquid that it ruptures. This mode is likely to be operative in the trachea and larger airways.

The deposited-film transport regime occurs after plug rupture or direct coating. The resulting film coating the airways will flow from combinations of gravity, airflow shear effects, and surface tension, and these effects may compete depending on the system parameters. This mode is probably dominant in the large-to-medium-sized airways.

When the liquid and its constituents (such as surfactant) form a surface layer, then surface-tension gradients (when present) become significant whenever gravity and capillarity are weak, as is the case in thin layers. These gradients cause Marangoni flows that distribute the surfactant. This regime is likely to be present in the medium-to-small airways. The fundamental fluid mechanics and transport phenomena of surface-layer surfactant spreading were reviewed in Refs. 26 and 27. The available theoretical models of the Marangoni flow on thin, viscous films are based on lubrication theory (5, 16, 22, 28, 31, 42, 43, 45, 71), from which coupled evolution equations for the film depth and the surfactant concentration are derived. If the surfactant is localized on an otherwise clean interface (Fig. 1*A*), the unsteady spreading flow generates a wave that travels in the direction of lower surfactant concentration (higher surface tension) (Fig. 1*B*). If surface diffusion of the monolayer and gravity are negligible, the wave behaves like a shock wave, with rapid changes in height and surface-tension gradients over a very short distance. The film thickens to twice its undisturbed

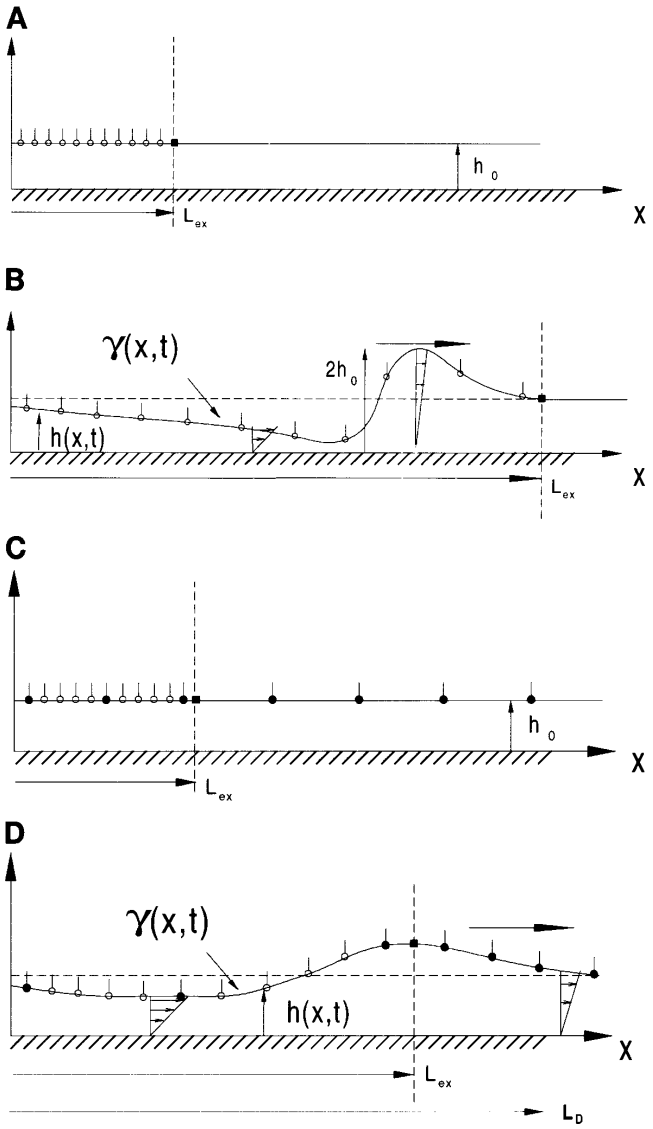

Fig. 1. *A*: surfactant monolayer on a uniform clean film of height h_0 before spreading, at time $t = 0$. L_{ex} denotes position of leading edge of exogenous surfactant. *B*: surfactant spreading on a deforming interface, where $h(x,t)$ is the film height and $\gamma(x,t)$ is surfactant concentration at a distance x from trachea and at $t > 0$. *C*: surfactant monolayer on a contaminated film before spreading begins, where exogenous surfactant is depicted with ○ and endogenous surfactant with ●. *D*: effect of preexisting endogenous surfactant on film deformation, surfactant distribution, and position of L_{ex} front with respect to leading edge of compression wave L_D. See *Glossary* for other definitions.

height at the traveling shock, and the film thins significantly behind it, so much so that it may rupture there (21, 42). Film rupture causes the spreading to stop, an unwanted result for SRT. The speed of this advancing shock wave depends on the surface-tension difference driving the flow, the film thickness, the surfactant activity, and the fluid viscosity.

In physiological applications, there is a preexisting or background surfactant already on the interface before exogenous surfactant is added. It may arise from natural (endogenous) sources or from previous SRT treatments. If the surfactant is localized on an interface with preexisting surfactant (Fig. 1, *C* and *D*), the leading edge of the new exogenous material (L_{ex}), spreads more slowly because of the background surfactant (28). This is due to the smaller surface-tension gradients. However, a second phenomenon arises: compression of the background surfactant as the exogenous surfactant spreads. This compression wave causes the background surfactant particles to move closer together, i.e., to increase in concentration, and the wave speed is faster than the spreading speed of the exogenous surfactant. Thus the leading edge of the compression wave (L_D) travels ahead of L_{ex} (Fig. 1*D*). For larger initial background concentrations, the compression speed actually increases because of greater mobility in the interface while the spreading speed decreases. These phenomena were presented and discussed in Ref. 28.

Components within the liquid (surfactants, drugs) may reach the alveolar compartment where the transport conditions may include removal and production kinetics. The clearance mechanisms for instilled surfactants, both lipid and protein fractions, are not entirely understood, although several studies have addressed some of the key issues (80). Alveolar type II cells appear to take in the vast majority (7, 64) and can recycle a portion for secretion. Minor amounts appear to be taken up by alveolar macrophages and bronchial Clara cells (7, 60). A few percent exits by the proximal airway (61). Treatment doses of surfactant are often as much as ten times the endogenous pool of surfactant. There have been a number of clearance studies examining recovery of radiolabeled surfactant from alveolar wash or lung tissue. Although several early papers have viewed surfactant as being cleared at a fixed percentage (of the initial mass) per hour (19, 60, 62, 68), it has become more clear that the kinetics is first order (63, 64). It has been shown that clearance rates can be modified if there is lung injury. For example, it was found by Novotny et al. (59) that clearance rates for adult rabbit lungs with prolonged 100% oxygen exposure were lowered. Such changes become important in determining dosing regimens for the injured lung, as may occur in ARDS. Also, some acute injuries may not affect clearance. The acute lung injury models shown in Refs. 35 and 52 were made with injections of *N*-nitroso-*N*-methylurethane. Clearance of instilled surfactant was similar to that in controls (52), there was altered endogenous surfactant metabolism in response to surfactant treatment in the injured animals, and exogenous surfactant was beneficial to the injured animals (35).

In an earlier study (44), we examined surfactant spreading in a lung model based on Marangoni flow alone. That model allowed for the rapid increase in airway surface area due to airway branching, which can quickly dilute the spreading surfactant. This surface-area dilution reduces the Marangoni mechanism locally and dramatically slows the process: transit times of the order of 2–3 h for an adult and 10–20 min for an infant were predicted by using zero flux end conditions. In the present work, we extend and improve this model to account for the other three transport regimes mentioned above. The model remains one dimensional, so that much of the geometric complexity of the bronchial tree is ignored, although the salient geometric features are retained. We shall estimate transit times and the time required for essentially complete delivery of the surfactant dose to the alveoli. How these transport times depend on the system parameters will be a main focus of the work. Through this modeling, we seek to develop an understanding of the fluid mechanics and transport of liquid delivery into the lung. Such an approach to overall lung transport for instilled liquid delivery, including exogenous surfactants, can provide a rational basis for developing strategies to optimize their delivery.

FORMULATION OF THE MODEL

Glossary

It will be useful and instructive to cast several of our variables in dimensional terms and in their dimensionless counterparts. We shall adopt the convention of using lowercase symbols to denote dimensional variables and uppercase symbols to denote their dimensionless version.

α	Fraction of fluid in draining region
a, A	Total airway cross-sectional area
a_e	Total airway cross-sectional area exposed to air
a_n	Total cross-sectional area at generation n
a_0	Tracheal cross-sectional area
A_A	Total alveolar surface area
A_{tr}	Cross-sectional area of endotracheal tube
b, B	Total airway perimeter
$\hat{B}$	Scaled perimeter function used in Marangoni flow regime
b_n	Total airway perimeter at generation n
b_0	Tracheal perimeter
β	Perimeter parameter
Ca	Capillary number
Ca_{tr}	Tracheal capillary number
d_n	Mean airway diameter at generation n
d, D	Airway diameter
d_0	Tracheal diameter
Δ	Airway taper parameter
$\Delta\sigma_n$	Surface-tension difference over length l_n
F	Ratio of surfactant delivery to the alveolar space to the rate of uptake

$\hat{F}$	Rescaled delivery of surfactant-to-uptake ratio
g	Gravitational acceleration
G	Ratio of typical gravity draining speed to Marangoni speed
$\gamma, \Gamma, \hat{\Gamma}$	Surfactant concentration
γ_A, Γ_A	Alveolar surfactant concentration
Γ_{eq}	Equilibrium alveolar surfactant concentration
$\hat{\Gamma}_{eq}$	Equilibrium surfactant concentration in Marangoni flow regime
$h, H, \hat{H}$	Film depth
H_{eq}	Equilibrium film thickness in the Marangoni regime
H_M	Critical film thickness for transition from gravity to Marangoni regimes
h_n	Liquid lining thickness at generation n
K	Rate constant for alveolar surfactant uptake
l_n	Mean airway length of generation n
l_0	Tracheal length
L_D	Leading edge of surface-compression wave
L_{ex}	Leading edge of exogenous surfactant
L_M	Marangoni regime length
L_0	Total airway path length
λ	Leading edge of bolus draining under gravity
Λ	Ratio of tracheal length to four times the path length
m, M	Mass of exogenous surfactant delivered to the alveoli
m_{dose}	Dose of surfactant delivered
μ	Fluid viscosity
n	Airway generation number
N_A	Avogadro's number
n_r	Critical generation number for plug rupture
p_A, P_A	Alveolar surfactant production rate
q, Q	Surfactant flux and fluid volume flux in Marangoni regime
q_a, Q_A	Surfactant flux into the alveolar compartment
$r, R, \hat{R}$	Airway radius
r_n	Mean airway radius at generation n
r_0	Tracheal radius
ρ	Liquid density
S_M	Surface-tension difference across the Marangoni regime
S_0	Surface-tension difference along the surface layer
σ	Surface tension
σ_n	Surface tension at generation n
t	Time
T	Dimensionless time used for deposited film flow
T_α	Transit time for gravity-driven flow
T_I	Inspiration time
T_M	Marangoni time scale
$\hat{T}_s$	Surfactant transit time at steady state
$\hat{T}$	Dimensionless time for surface-layer transport
τ	Alveolar uptake time variable
τ_D	Exogenous surfactant delivery time
θ	Surfactant activity parameter
ϕ	Film thickness correlation function
U	Speed of propagation of liquid plug
U_g	Typical speed of gravity-driven drainage
U_M	Marangoni velocity scale
$\hat{U}_s$	Marangoni velocity at air-liquid interface
U_{tr}	Tracheal velocity scale
v, V	Liquid bolus volume
V_b	Initial bolus volume
$\dot{V}$	Airflow rate
V_p	Initial liquid plug volume
V_T	Tidal volume
V_{tr}	Tracheal volume
W_b	Ratio of bolus volume to tracheal volume
W_p	Ratio of initial plug volume to tracheal volume
W_r	Value of W_p that will rupture at generation n
x, X	Distance along fluid layer, measured from the tracheal carina
$\hat{X}$	Dimensionless distance along fluid layer starting at *generation 7*
$\hat{X}_a$	Size of domain of Marangoni regime
x_n, X_n	Distance along fluid layer to generation n
ξ_1, ξ_2	Initial condition parameters for surface-layer flow

Lung morphometry. The transport models we develop require as input a mathematical description of airway geometry. We have employed the model used in Ref. 76, which assumes that the adult lung is a symmetric, dichotomous branching tree, in which the mean length of an airway is proportional to its diameter and for which the airway volume for each generation is constant. According to this model, the number of airways at generation n is 2^n, for $0 \le n \le 23$, and the mean airway diameter (radius) is d_n (r_n), the mean airway length is l_n, the total cross-sectional area of the airways is a_n, the total airway perimeter is b_n, given respectively by

$$d_n = d_0 2^{-n/3}, \qquad r_n = r_0 2^{-n/3},$$
$$l_n = l_0 2^{-n/3}, \qquad a_n = a_0 2^{n/3}, \qquad b_n = b_0 2^{2n/3} \tag{1}$$

Here, d_0 (r_0), l_0, a_0, and b_0 represent the tracheal diameter (radius), length, cross-sectional area, and perimeter, respectively. The tracheal values from Ref. 76 are $d_0 = 1.8$ cm and $l_0 = 12$ cm, from which r_0, a_0, and b_0 may be computed. The distance from the tracheal carina to the end of generation n is denoted by the discrete variable, x_n. It may be expressed as the sum of the intervening airway lengths l_n, as given in *Eq. 1*. This geometric sum yields a simpler form

$$x_n = -l_0 + \sum_{m=0}^{n} l_m = L_0(1 - 2^{-n/3}) \tag{2}$$

where the total path length is $L_0 = l_0/(2^{1/3} - 1) \approx 15$ cm in the adult. Using *Eq. 2*, we eliminate n from *Eq. 1* and replace the discrete variable x_n with the continuous variable x. Then the functions in *Eq. 1* become continuous functions of x. These are further simplified by representing them in dimensionless form as follows

$$D(X) = \frac{d(x)}{d_0} = (1 - X), \quad R(X) = \frac{r(x)}{r_0} = (1 - X)$$
$$A(X) = \frac{a(x)}{a_0} = (1 - X)^{-1}, \quad B(X) = \frac{b(x)}{b_0} = (1 - X)^{-2} \tag{3}$$

where the dimensionless pathway distance is now $X = x/L_0$, and we note that $0 \leq X < 1$. Upper (lower) case variables are used to indicate nondimensional (dimensional) variables. The introduction of continuous variables and functions will allow us to apply conservation equations for mass and momentum as they arise in the analyses.

For example, using the above formulation, the path distance to the beginning of *generation 9* is $X_9 = x_9/L_0 = 1 - 2^{-3} = 0.875$. At that location, the airway diameter (radius) is 0.125 times the tracheal diameter (radius), the cross-sectional area is 8 times the tracheal cross-sectional area, and the total airway perimeter is 64 times the tracheal perimeter. The beginning of the alveolated region of the lung can be represented by *generation 18*, say, which is at $X_{18} = x_{18}/L_0 = 1 - 2^{-6} = 0.984$. We use this value as our boundary with the alveoli, so that the singularities in $A(X)$ and $B(X)$ as $X \rightarrow 1$ (see *Eq. 3*) are always avoided. The Weibel model describes the mean diameter of the first 10 generations reasonably accurately but underpredicts the diameter for generations beyond $n = 10$ and overestimates the number of airways at large n (77). The derived formula for distance along the path as a function of airway generation, *Eq. 2*, approximates measurements of path length (29, 75) within a few percent, except for *generations 1* and *2* where the error is larger. No allowance is made for asymmetry in airway branching. However, we use this model to keep the analysis relatively simple. Employment of more sophisticated functions of X will be possible in future studies.

In the Weibel model (76), the pulmonary tree is self-similar, so that the scaling relationship between adjacent airway generations is independent of generation number. It is, therefore, possible to employ the same functional forms for $D(X)$, $R(X)$, $A(X)$, and $B(X)$ to represent truncated portions of the pulmonary tree, although the reference path length L_0, the reference perimeter b_0, and the X range of interest must be redefined appropriately. This is particularly useful for representing infant lung morphometry, necessary for predictions of liquid and surfactant transport in our analyses. We assume for simplicity that the neonatal lung may be modeled by equating the neonatal trachea to the adult *generation 7* airway, and then use the distal adult lung section, $7 \leq n \leq 18$, as the remaining neonatal lung. Therefore, the neonatal trachea diameter is equivalent to $d_7 = 0.36$ cm according to *Eq. 1*, a value typical for premature infants. Then the reference quantities in *Eq. 3* would be replaced by the *generation 7* values for a single airway, i.e., d_7 replaces d_0, r_7 replaces r_0, πd_7 replaces b_0, and πr_7^2 replaces a_0. Then L_0 in *Eq. 2* must be replaced by $2^{-7/3} L_0 = 3.75$ cm, which is the neonatal total path length.

We now present some analyses of the four transport regimes: liquid plug, deposited film, surface layer, and alveolar compartment. For delivery of surfactants, for example, we shall see that the liquid plug flow and the initial drainage of a deposited film due to gravity occur on the order of seconds. The ultimate delivery of the surfactant to the alveoli is governed by a balance of surfactant supply along the surface layer and surfactant uptake in the alveolar compartment, which occurs on the order of hours. The details of the first two regimes are given to demonstrate the relevant transport mechanisms. The initial distribution of surfactant from these relatively rapid events then provides input to the second two regimes.

Liquid plug flow. After a liquid bolus of surfactant is delivered into the trachea, it may be large enough to occlude the airway. If so, it will initially be pushed into the distal regions of the lung by the ventilatory airflow. As this liquid plug propagates through the tracheobronchial tree, driven by a constant airflow rate $\dot{V}$, it leaves behind a trailing liquid film of thickness h coating the airway (see Fig. 2*A*). As long as it is not picking up comparable amounts of liquid from the airway wall ahead, the size of the plug will diminish until it ruptures (Fig. 2*B*). More complex situations involving airway liquid linings, which are comparable in thickness to the trailing film and in which airway flexibility

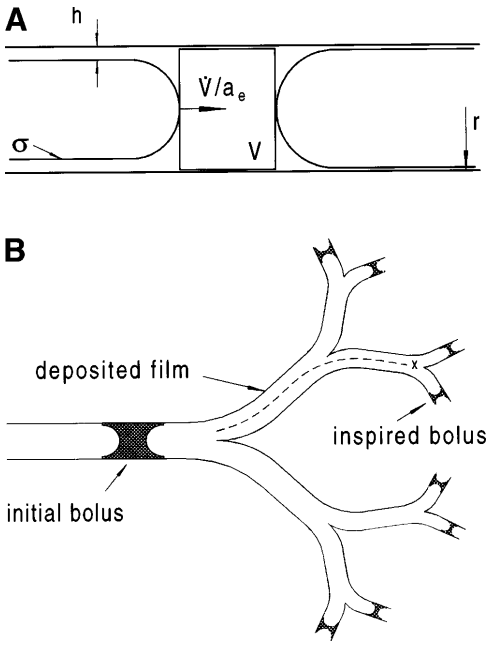

Fig. 2. *A*: liquid plug of volume (V) propagating down an airway of radius (r) due to airflow rate ($\dot{V}$), leaving behind a trailing film of thickness (h). *B*: progression of liquid plug through a symmetric airway network illustrating loss of volume as it travels from trachea to *generation 3*. See *Glossary* for other definitions.

is important, are not treated here. An estimate of how far a liquid plug travels through the lung before it ruptures is made by using simple mass-conservation arguments. The change of plug volume v, with respect to distance x, is given by

$$\frac{dv}{dx} = -[a(x) - a_e(x)] = -bh\left(1 - \frac{h}{2r}\right) \qquad (4)$$

where $a_e(x)$ is the total cross-sectional area seen by the gas flow behind the plug. Note that $a_e(x)$ is smaller than the total airway cross-sectional area $a(x)$, due to the deposited liquid film.

This type of flow has been studied by previous investigators who examine the motion of long bubbles in tubes (6, 70). Their results indicate that the ratio of deposited film thickness to airway radius, $H = h/r$, depends on the capillary number, $Ca = \mu\dot{V}/(\sigma a_e)$, which is a dimensionless airflow speed. Here, μ is the fluid's viscosity, and σ is its surface tension (assumed for the present to be constant). Note that Ca is a decreasing function of x, since a_e increases with x. It is convenient to relate the variable Ca to its tracheal value Ca_{tr}, such that

$$Ca(X) = Ca_{tr}\frac{(1 - X)}{(1 - H)^2} \qquad (5)$$

where $Ca_{tr} = \mu\dot{V}/(\sigma a_0)$. H may be obtained by curve-fitting the results of a numerical analysis for bubbles advancing along tubes (D. Halpern, unpublished observations), which is similar to our previous theoretical work on such flows in channels (30)

$$H = \phi(Ca) = 0.36(1 - e^{-2Ca^{0.523}}) \qquad (6)$$

This function of H asymptotes to the value 0.36 in the limit $Ca \rightarrow \infty$. As a practical matter, $H \approx 0.36$ when $Ca > 4.0$. In the other limit, as $Ca << 1$, $H \approx 0.72Ca^{0.523}$. Both of these limits are consistent with the previous literature (55, 70). Inserting *Eq. 3* into *Eq. 4* and integrating with respect to X yields the dimensionless plug volume distributed across the airway generation at X

$$V(X) = \frac{v(x)}{V_p} = 1 - \frac{1}{2W_p\Lambda}\int_0^X \frac{\phi(1 - \phi/2)}{1 - X}\,dX \qquad (7)$$

where ϕ depends on X, according to *Eqs. 5* and *6*, $W_p = V_p/V_{tr}$ is the ratio of the initial plug volume to tracheal volume, $V_{tr} = \pi r_0^2 l_0$, and $\Lambda = l_0/(4L_0)$. The plug ruptures when $V(X) = 0$. This occurs if Ca_{tr} is large enough or if W_p is sufficiently small for the right-hand side of *Eq. 7* to reach zero at some $X < 1$.

A liquid plug in the airways can only proceed distally if it is inflating the lung region ahead of it. Blowing a plug into the airways, as discussed above, accomplishes this. Gravity, on the other hand, is not likely to provide enough force for the distal motion of an intact liquid plug. However, gravity can disrupt its motion and cause it to drain along the walls.

It is important to consider under what conditions a liquid plug is formed during tracheal instillation. Experimental studies of the criteria for plug formation during instillation have been presented in the work of Espinosa and Kamm (15), for example, in which effects of flow speed and duration, along with fluid properties, are examined. For the purposes intended here, we shall consider an initial liquid bolus instilled into the trachea as immediately coating the tracheal wall uniformly. Then the pertinent issue becomes what liquid bolus volume, when delivered into the trachea, would be large enough to form a liquid plug. From stability studies of liquid-lined tubes (17, 32, 33, 47), a uniform film coating the walls will form a plug when the liquid-film thickness divided by the tube radius H is roughly $>0.12–0.16$. The range depends mainly on the surfactant concentration, its strength or activity, the tube length, and the relative wall flexibility (33). Once the film becomes unstable, it will quickly form a plug over a time interval on the order of $\mu r/\sigma$ (34), which is much shorter than 1 s over a wide range of parameter values. From simple volume calculations, the film's initial thickness in the trachea is

$$H = 1 - (1 - W_b)^{1/2} \qquad (8)$$

where W_b is the ratio of bolus volume to tracheal volume. Clearly $H = 1$ when $W_b = 1$ and the trachea is completely filled. For a tracheal plug not to form, we could seek a criterion that $H \leq 0.1$, which occurs whenever $W_b \leq 0.19$. For a tracheal plug to form, we could specify that $0.2 \leq H \leq 1$, which occurs when $0.36 \leq W_b \leq 1$, and this would be the range where $W_p = W_b$, i.e., the initial bolus volume becomes the initial plug volume.

A significant issue in the practical aspects of surfactant and liquid delivery into the lung is the regurgitation, or reflux, of material out of the trachea following instillation. One potential explanation of this phenomenon is related to the criterion for plug formation discussed above. For any airway, not just the trachea, if the liquid lining becomes too thick, i.e., $H \geq 0.2$, then it will form a plug, given sufficient time. As the tracheal plug is blown distally during inspiration, the trailing film thickness may exceed this criterion in some airway generations that will be subject to formation of their own plugs. Depending on which airway generation is involved and when this happens in the respiratory cycle, these newly formed plugs may be convected out of the trachea during expiration. The clinician who encounters reflux may respond by trying to blow in the tracheal bolus more forcefully with the intent of quickly pushing it to the alveolar region. Our model indicates that this approach could be counterproductive, since the reflux may be a result of a newly formed plug and not the original plug, which could have reached the distal parts of the lungs. Also, more forceful delivery implies a larger Ca and, hence, a thicker film.

Deposited-film flow. The advancing plug leaves behind itself a film of thickness h. Once the plug ruptures, this trailing film contains the liquids or surfactants that may need to reach the alveoli. The transport of this

film then becomes an important issue. Here, we want to determine whether this film flow is dominated by gravity or by Marangoni forces. Although airways are oriented in many different directions, clinically, the patient may be positioned at several angles during the delivery process, so that the majority of airways may experience appreciable gravitational forces directed distally.

The speed of gravity-driven drainage of the liquid lining in a single airway generation n is approximately $U_g = \rho g h_n^2/(3\mu)$ (1), where ρ is the liquid density, g is the gravitational constant, and h_n is the liquid lining thickness at generation n. By comparison, if the same thin fluid layer is subject to a surface-tension gradient of magnitude $\Delta\sigma_n/l_n$, where a surface-tension difference $\Delta\sigma_n$ is felt over the distance l_n and the flow has average speed $U_M = \Delta\sigma_n h_n/(2\mu l_n)$ (42) due to Marangoni forces. Both of these velocities are proportional to μ^{-1}, but U_g has a quadratic dependence on the film thickness h_n, whereas U_M has a linear dependence. We, therefore, expect surface-tension gradients to dominate the film flow as the film thickness decreases. Let the parameter $G = U_g/U_M = 2\rho g h_n l_n/(3\Delta\sigma_n)$ represent the ratio of these speeds. If $G >> 1$, spreading of the deposited film may be gravity dominated; when $G << 1$, surface-tension gradients, Marangoni flows, may be dominant. The two flow mechanisms are, therefore, of comparable magnitude when $G \approx 1$ or when $h_n = H_M$, where

$$H_M \approx \frac{3S_0}{2\rho g L_0} \qquad (9)$$

$\Delta\sigma_n/l_n$ has been replaced by the average estimate for the whole domain, S_0/L_0 (S_0 represents the surface tension difference between the trachea and the alveoli). This relation defines a critical film thickness for the deposited film, above which gravitational forces may be dominant and beneath which surface-tension gradients may be dominant.

We can estimate the magnitude of H_M for delivery of a liquid bolus to an adult lung by taking $\rho \approx 1$ g/cm^3; $g \approx 10^3$ cm/s^2, and $S_0 \approx 50$ dyn/cm. This surface tension difference is initially distributed across the path length $L_0 \approx 15$ cm, yielding $H_M = 50$ μm. As shown later, for typical ventilation rates and tracheal plug volumes in an adult, the trailing film reaches this value of H_M near *generation 7*. For a neonate, the initial surface-tension gradient is distributed over a length of only 3.75 cm, so $H_M = 200$ μm. This value of H_M is 11% of the tracheal radius, a value that may lead to plug formation. Then transport will, again, be dominated by airflow.

We first consider the gravity-driven drainage regime in an adult. For simplicity, we are considering that the deposition by the liquid bolus occurs first, followed by drainage. It is helpful to consider two extreme cases. One case is when the instilled bolus forms a plug in the trachea and it ruptures in the trachea. Equivalently, this starting condition could be achieved by direct deposit of the initial liquid bolus on the tracheal walls. Either way, this would leave the entire bolus volume to drain from the trachea to the distal airways. The other case is when the plug ruptures or persists in the alveolus, leaving a coating over all airways.

If the bolus ruptures in the trachea, then the initial bolus volume V_b drains unsteadily and nonuniformly down the airway walls (see Fig. 3). We model this process, by extending existing theories (40, 57) of flow down a vertical surface to include the increase of surface perimeter $B(X)$ (see *Eq. 3*), along the draining axis, as occurs in the lung. Applying conservation equations for mass and momentum for lubrication flow, the resulting evolution equation for the dimensionless film thickness $H(X,T)$ is found to be

$$(BRH)_T + (BR^3H^3)_X = 0 \qquad (10)$$

where the dimensionless time variable is $T = \rho g r_0^2 t/(3\mu L_0)$. A solution of *Eq. 10* for the evolving film thickness $H(X,T)$ is

$$H(X, T) = [(1 - X)T]^{-1/2}$$
$$\text{for } 0 \le X \le \lambda(T) = 1 - [1 + \Lambda W_b T^{1/2}]^{-2} \qquad (11)$$
$$H(X, T) = 0 \qquad \text{for } X > \lambda(T)$$

For an adult, $\Lambda = 0.2$, whereas for a neonate $\Lambda = 0.16$. $H(X,T)$ has a sharp front at the film's leading edge located at $X = \lambda(T)$. This analysis tells us the drainage front speed and the thickness of the film behind this front. The thinnest value of h, ($h = rH$), is at the front, so when it is comparable to H_M (see *Eq. 9*), Marangoni forces become important for transport in the surface-film regime. This solution in *Eq. 11* may then also be used to calculate the amount of time required for all of the deposited film to drain past a certain airway generation. Whereas the front may take only seconds to reach *generation 7*, for example, it may take many hours for all of the remaining liquid to drain past *generation 7*. Calculations for the front-arrival time and the liquid-drainage time are given below.

The other extreme case is when the plug ruptures or persists at the alveolar level. Now there is liquid

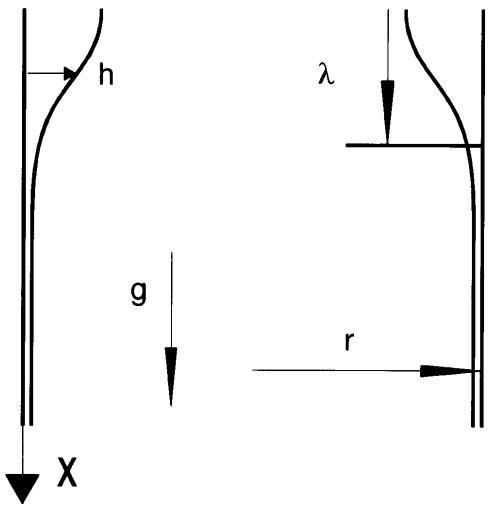

Fig. 3. Liquid bolus of thickness h draining due to gravity on a vertical wall. Leading edge of bolus is denoted by $X = \lambda$. See *Glossary* for other definitions.

deposited between *generations 0* and *18*. Because $H(X,T)$ in *Eq. 11* is a similarity solution, eventually, the deposited liquid is likely to evolve to this distribution. Now the appropriate range of t is for times greater than the time to rupture. So we see that the two extremes yield similar features: front transit on the order of seconds, and further drainage of the liquid lining on the order of hours.

Surface-layer transport. Surface-tension effects dominate spreading once the film becomes sufficiently thin, as shown in the previous section. We examine two types of surface-tension-driven flows: Marangoni flow driven by surface-tension gradients (Fig. 1) and flows driven by axially varying pressure gradients associated with nonuniform curvature of tapering airways. The analysis (given in APPENDIX) shows that Marangoni flows are eventually much stronger than those due to nonuniform curvature. Both the initial rapid transient behavior of these flows and their subsequent steady states are considered.

The unsteady, transient flow created by the surface-tension gradients, although short-lived, is important to understand, since it may cause certain undesirable events to occur. For example, as the flow is initiated, the airway liquid-lining thickness, $\hat{H}(\hat{X},\hat{T}) = h(x,t)/h_7$ and the surfactant concentration, $\hat{\Gamma}(\hat{X},\hat{T}) = \gamma(x,t)/\gamma_7$, change as functions of $\hat{X}$ and $\hat{T}$, where the hat over the variables indicates new scalings that better represent the Marangoni regime (see APPENDIX). The h_7 is the reference film thickness at *generation 7* in the adult. The surface-tension difference between *generations 7* and *18* is $S_M = \sigma_{18} - \sigma_7 = -\theta\,(\gamma_{18} - \gamma_7)$, where the surfactant activity θ represents the surface-tension-reducing capacity of the monolayer and is taken to be constant. This is equivalent to assuming a linear equation of state for the surface tension-surface concentration relationship. The scaling for the axial variable is the Marangoni regime length, $L_M = x_{18} - x_7$, and the scaling for time is $T_M = \mu L_M^2/S_M h_7$, which is characteristic of Marangoni flow over the distance L_M, so that $\hat{X} = x/L_M$ and $\hat{T} = t/T_M$.

Conservation of mass and momentum lead to the governing equations for $\hat{H}$ and $\hat{\Gamma}$, *Eq. A1* in APPENDIX. These include the parameter Δ, representing the effects of surface-tension-driven flows due to airway taper. The equations are solved numerically in the domain $0 \le \hat{X} \le \hat{X}_a$, which corresponds to the pathway segment from the beginning of *generation 7* to the beginning of *generation 18*, where the alveolar boundary is located. If the lining becomes too thin at a particular value of $\hat{X}$, it may rupture there because of destabilizing van der Waals forces, i.e., $\hat{H} = 0$, which may lead to a cessation of spreading (42). However, if $\hat{H}$ becomes too large, then there may be plug formation, as discussed above, which will also stop spreading. Before examining the effects of surface-area expansion, we consider an unsteady solution of *Eq. A1* for $\hat{H}$ and $\hat{\Gamma}$ for a single, uniform tube.

Figure 4 shows the time evolution of $\hat{H}$ and $\hat{\Gamma}$ for the case of a single, uniform tube with the upstream and downstream surfactant concentrations fixed at $\hat{\Gamma}\,(\hat{X} = 0,\hat{T}) = 1$ and $\hat{\Gamma}\,(\hat{X} = \hat{X}_a,\hat{T}) = \Gamma_A = 0.2$, respectively,

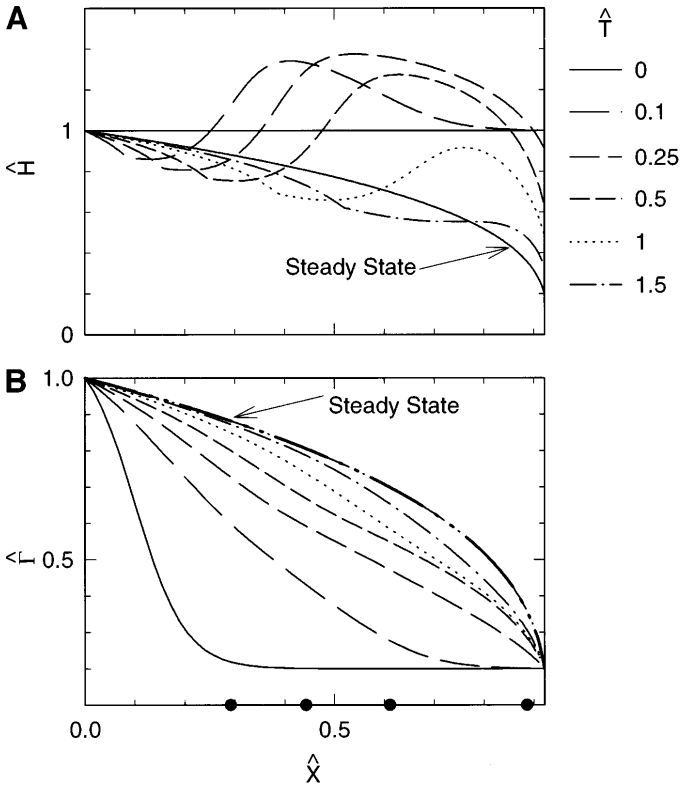

Fig. 4. $\hat{H}(\hat{X},\hat{T})$ (*A*) and $\hat{\Gamma}(\hat{X},\hat{T})$ (*B*) vs. $\hat{X}$ at $\hat{T} = 0$, 0.1, 0.25, 0.5, 1, and 1.5 for spreading with no surface-area expansion or curvature effects (total airway perimeter $B = 1$, $\Delta = 0$) and an initially flat film with $\Gamma_A = 0.2$. ● in *B* show leading edge of exogenous surfactant distribution at times 0, 0.1, 0.25, 0.5. See *Glossary* for other definitions.

where $\Gamma_A = \gamma_A/\gamma_7$. The initial conditions for $\hat{H}$ and $\hat{\Gamma}$ are discussed in the APPENDIX. Shear stresses from the initially large negative gradient in surfactant concentration drive a flow in the $\hat{X}$ direction, causing the fluid layer to well up behind the leading edge of the advancing disturbance (e.g., at $\hat{T} = 0.1$). As the monolayer advances, the disturbance first grows and then diminishes in size. At $\hat{T} \approx 2$, the leading edge of the disturbance in $\hat{\Gamma}$ reaches $\hat{X} = \hat{X}_a$, and a nonzero surfactant gradient is established there. This surfactant gradient increases and induces film thinning at the downstream end until $\hat{T} \approx 4$, when the fluxes of surfactant at $\hat{X} = 0$ and $\hat{X} = \hat{X}_a$ equalize, and $\hat{\Gamma}$ has essentially reached a steady state. The $\hat{H}$ distribution evolves for a slightly longer time. These steady solutions are obtained by setting $\hat{\Gamma}_{\hat{T}} = \hat{H}_{\hat{T}} = 0$ in *Eq. A1*, which can be integrated to yield

$$\hat{\Gamma}(\hat{X}) = \hat{H}(\hat{X}) = [1 - (1 - \Gamma_A^3)\hat{X}]^{1/3}, \quad 0 < \hat{X} < \hat{X}_a \qquad (12)$$

These solutions resemble the steady solutions for the case $\Gamma_A = 0$ given by Ref. 12.

The leading edge of the exogenous surfactant distribution, shown by the black markers in Fig. 4*B*, takes approximately half a time unit to reach the downstream end, significantly longer than the time taken for the disturbance first to reach $\hat{X} = \hat{X}_a$. As was shown in Ref. 28, an increase in Γ_A causes the transit time of

exogenous surfactant to increase, since the surface-tension gradient driving the flow is reduced.

The effect of the lung's surface-area expansion on the unsteady spreading of surfactant is shown in Fig. 5. $\hat{H}$ and $\hat{\Gamma}$ are plotted as functions of $\hat{X}$ (on a logarithmic scale) and the equivalent generation number n. Pressure-driven flows due to changes in airway radius are neglected for the time being. As $\hat{H}(\hat{X},\hat{T})$ in Fig. 5*A* evolves from the initial conditions (given in APPENDIX), a kinematic wave propagates from left to right (as in Fig. 4*A*), with thinning occurring at the upstream end of the domain. After the wave reaches the downstream end, the film begins to thicken, and the wave is damped. Compared with Fig. 4*B*, the leading edge of the surfactant front in Fig. 5*B* progresses to the distal airways more slowly because surfactant has to distribute itself over an expanding surface area and also because the initial film thickness (given by *Eq. A4*) is thinner than that used in Fig. 4. At $\hat{T} = 0.6$, a nonzero surfactant flux at the downstream end is established, which is weaker than the uniform-tube case. Whereas the surfactant concentration increases monotonically with time at fixed $\hat{X}$ in the uniform tube (Fig. 4*B*), this is not the case (Fig. 5, *B* and *C*) for an expanding surface area. When the disturbance first reaches the downstream end of the domain, the fluid layer is relatively thin, so that large shear stresses are needed to drive the flow ($\hat{T} = 1$, 2), and, hence, $\hat{\Gamma}$ rises to relatively high values in *generations 13–17* (Fig. 5*C*). Later, as fluid is driven distally and the liquid layer thickens in this region (Fig. 5*A*), the viscous resistance to flow falls and the surfactant gradients fall also, causing $\hat{\Gamma}$ to fall ($\hat{T} \geq 4$).

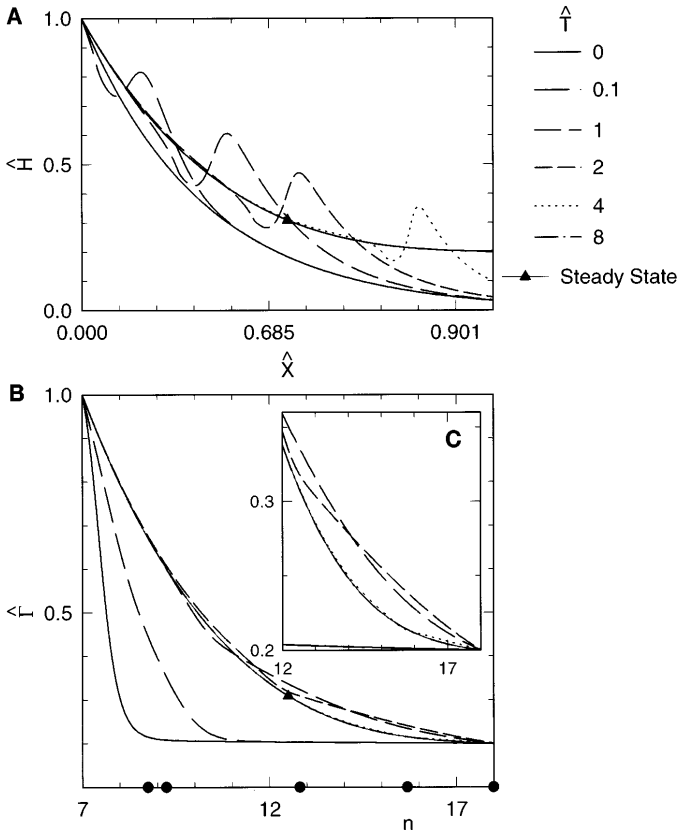

Fig. 5. $\hat{H}(\hat{X},\hat{T})$ vs. $\hat{X}$ on a logarithmic scale (*A*) and $\hat{\Gamma}(\hat{X},\hat{T})$ vs. generation number n at $\hat{T} = 0$, 0.1, 1, 2, 4, and 8 (*B*, *C*), incorporating effects of surface-area expansion, obtained by solving *Eq. 1A* with $\Gamma_A = 0.2$ and $\Delta = 0$. Solid curves with symbols show ultimate steady state; ● in *B* show leading edge of exogenous surfactant distribution at times 0, 0.1, 1, 2, and 3.07. See *Glossary* for other definitions.

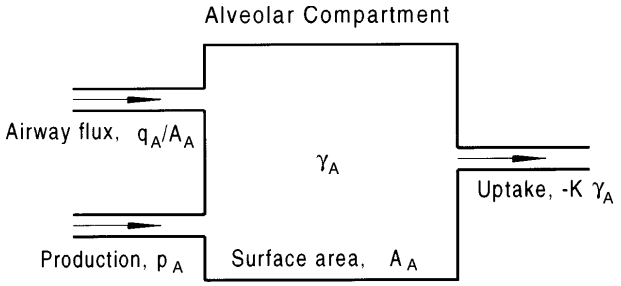

Fig. 6. First-order alveolar compartmental model, indicating that alveolar surfactant concentration γ_A increases due to alveolar production p_A and airway surfactant flux q_A but decreases due to constant rate of uptake K.

A steady state is reached once $\hat{T} \approx 7$. Analytical steady-state solutions can be obtained from the governing equations (*Eq. A1*) and are given by

$$\hat{\Gamma}(\hat{X}) = \hat{H}(\hat{X}) = [1 - (1 - \Gamma_A^3) f(\hat{X})]^{1/3},$$

$$\text{where } f(\hat{X}) = \frac{1 - (1 - \hat{X})^3}{1 - (1 - \hat{X}_a)^3} \quad (13)$$

A comparison of the steady states plotted in Figs. 4*B* and 5*B* confirms that surface-area expansion dampens surface-tension gradients considerably. This is demonstrated by considering *Eqs. 12* and *13*, from which it can be shown that $|d\hat{\Gamma}/d\hat{X}|$ increases with $\hat{X}$ for the uniform tube but decreases monotonically with $\hat{X}$ for the surface-area-expansion lung model.

Alveolar compartment transport. When liquid and surfactant from the instilled bolus finally reach the alveolar region, alveolar surfactant kinetics begin to play a central role. As surfactant accumulates in the alveoli, the average concentration there, γ_A, will slowly rise and weaken the Marangoni flow. To determine the delivery time more accurately, a time-dependent model of alveolar surfactant uptake is developed. Treating the alveolar space as well mixed, the average surfactant concentration there can be modeled by using a simple model for the kinetics of alveolar surfactant (Fig. 6)

$$\frac{d\gamma_A}{dt} = \frac{q_A}{A_A} - K\,\gamma_A + p_A \quad (14)$$

where γ_A is the alveolar surface concentration of surfactant, q_A is the dimensional exogenous surfactant flux arriving at the alveolar compartment from the Marangoni flow, A_A is the total alveolar surface area exposed to the instilled bolus, K is the rate constant for surfactant uptake, and p_A is the alveolar surfactant production rate, which we take to be constant as a first approximation. This constant may be varied to represent different states of disease or recovery.

It appears that a half-life in the range of 5–15 h occurs for many of the surfactants used in alveolar-wash kinetics studies (60, 63, 64). Therefore, a reasonable estimate of the rate constant range is $0.046/h \leq K \leq 0.138/h$. It is convenient and instructive to recast *Eq. 14* in nondimensional terms. We define the nondimensional variables as follows: the time $\tau = Kt$, which is scaled on the uptake rate; the alveolar surfactant concentration $\Gamma_A = \gamma_A/\gamma_7$; the flux $Q_A = q_A/q_7$, such that $q_7 = \gamma_7 b_7 L_M/T_M$ and $P_A = p_A/(\gamma_7 K)$ is a parameter representing the ratio of natural surfactant supply to its uptake. Expressing *Eq. 14* in these nondimensional variables, we have

$$\frac{d\Gamma_A}{d\tau} = FQ_A - \Gamma_A + P_A \qquad (15)$$

where $F = (b_7 L_M)/(A_A K T_M)$ is a nondimensional parameter representing the ratio of the rate of delivery of surfactant to the alveolar space to the rate of uptake.

RESULTS

Liquid plug flow. As was shown in FORMULATION OF THE MODEL, *Liquid plug flow*, the volume of a liquid plug (*Eq. 7*) depends critically on the tracheal capillary number, Ca_{tr}, and on the ratio of initial plug volume to tracheal volume W_p. The adult tracheal volume is $V_{tr} = \pi r_0^2 l_0 = 30\ cm^3$, whereas a premature neonatal value is $V_{tr} = 2^{-7}\pi r_0^2 l_0 = 0.25\ cm^3$, roughly equivalent to the volume of a single adult *generation 7* airway. For neonates, a typical dose of surfactant liquid is two half-doses of 2.5 ml/kg. The first half-dose is instilled in small portions in time with each mechanical inspiration. Normally, the drug is administered over a 1- to 2-min period, corresponding to 30–50 mechanical breaths. Therefore, plug volumes may be $0.25\ cm^3$ or lower, so that $W_p \leq 1$. The range $W_p \leq 1$ is also reasonable for adults who experience instillation of surfactants, resuscitative drugs, or perfluorocarbons. Our analysis is not limited to $W_p \leq 1$; however, this is the range we will consider.

The airflow rate, $\dot{V}$, can be expressed in terms of the tidal volume V_T and an inspiration time T_I as $\dot{V} = V_T/T_I$. Defining a tracheal velocity scale to be $U_{tr} = V_T/(T_I A_{tr})$, where A_{tr} is the cross-sectional area of the endotracheal tube, the Ca_{tr} is then

$$Ca_{tr} = \frac{\mu}{\sigma} U_{tr} \qquad (16)$$

For a neonate, let the inner diameter of the endotracheal tube be 0.3 cm, which is slightly smaller than d_7, so that $A_{tr} = 0.07\ cm^2$. A typical value for inspiratory time, under conditions of assisted ventilation, would be $T_I = 0.7$ s, whereas a typical V_T could be $6\ cm^3$; then, $U_{tr} = 122$ cm/s. For an adult, $A_{tr} \approx \pi r_0^2 = 2.5\ cm^2$, $T_I \approx 2$ s, $V_T \approx 500\ cm^3$, yielding $U_{tr} = 100$ cm/s, approximately the same as the neonatal value. For either adult or neonate, the range of μ/σ depends only on the instilled substance. If that substance has a low surface tension, i.e., $\sigma = 5$ dyn/cm, and a high viscosity, i.e., $\mu = 0.6\ g\cdot cm^{-1}\cdot s$, or a high surface tension, i.e., $\sigma = 50$ dyn/cm, and a lower viscosity, i.e., $\mu = 0.01\ g\cdot cm^{-1}\cdot s$, then the range of μ/σ is roughly 2.0×10^{-4} s/cm $\leq \mu/\sigma \leq 0.12$ s/cm. For our representative value of $U_{tr} = 100$ cm/s, the range for the Ca_{tr} is $\sim 0.02 \leq Ca_{tr} \leq 12$.

In Fig. 7*A*, the plug volume given by *Eq. 7* is plotted vs. generation number for various values of W_p and Ca_{tr} that fall in the range calculated above. The plots show that the plug will rupture proximally for higher values of Ca_{tr} because the thickness of the deposited film is larger (see *Eq. 6*), and for smaller values of W_p, since there is less volume to distribute. Therefore, the generation number at which the plug ruptures decreases with decreasing W_p and increasing Ca_{tr}. From *Eq. 7* it is possible to compute the critical value of W_p (call it W_r) that will rupture at a specified generation number $n = n_r$. Figure 7*B* shows plots of W_r as a function of Ca_{tr} for selected values of n_r where clearly W_r increases with Ca_{tr} and airway generation. As shown in Fig. 7*A*, an increase in Ca_{tr} by a factor of 10, say from 1.2 to 12, does not have a significant effect on the deposited liquid distribution because of the asymptotic behavior of *Eq. 6*. If W_p is sufficiently large or Ca_{tr} is sufficiently small, then the liquid plug may not rupture in the airway domain. This could represent direct convection of instilled liquid into the alveolus. However, this is unlikely to occur, since there is always some gas trapped between the plug and the alveoli. The pressure in the gas would rise until the motion of the plug stopped somewhere proximal to the alveoli.

Direct instillation into the alveoli may be a desirable goal. Figure 8 is a plot of the alveolar plug volume, i.e.,

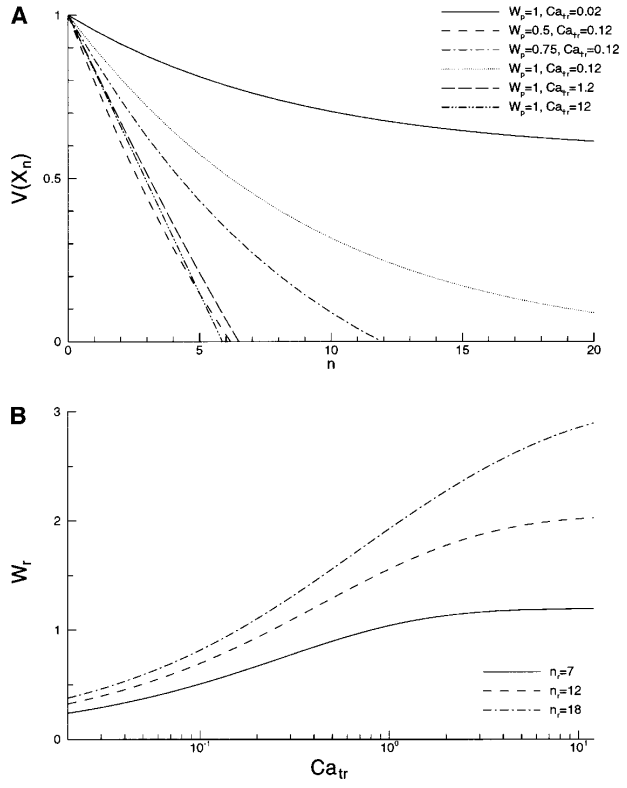

Fig. 7. *A*: liquid plug volume vs. airway generation *n* for a range of Ca_{tr} and W_p; *B*: critical plug volume that ruptures at *generation* n_r, W_r, vs. Ca_{tr} for $n_r = 7$, 12, and 18. See *Glossary* for definitions.

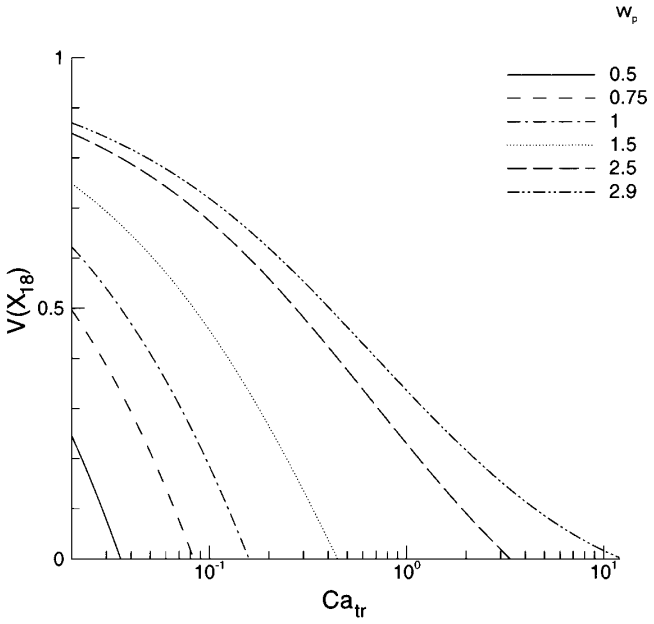

Fig. 8. Alveolar plug volume $V(X_{18})$ vs. tracheal capillary number Ca_{tr}, for various initial plug volumes W_p.

$V(X_{18})$ from *Eq. 7*, as a function of Ca_{tr} for several values of W_p. This figure shows that direct instillation into the alveoli is enhanced by larger volumes and smaller Ca_{tr}. As inferred from previous figures, the plug volume at *generation 18* decreases with increasing Ca_{tr} and decreasing W_p. For the range of parameters considered, rupture does not occur at *generation 18* (and earlier) if Ca_{tr} falls below 0.0035 and if $W_p \geq 0.5$. Also, the Ca_{tr} needed for rupture increases significantly if W_p is doubled, for example from 0.5 to 1.

From *Eq. 5*, as *Ca* increases, so does the thickness of the trailing film, *H* (see *Eq. 6*). This is illustrated in Fig. 9, where *H* is plotted as a function of airway-generation number *n* for several values of Ca_{tr} and W_p. It shows that for fixed Ca_{tr} and W_p, *H* is a decreasing function of *n*, since *Ca* decreases as the total cross-sectional area increases with *n*. *H* does not exceed 0.14, which is within the range necessary for closure, at any airway generation, provided Ca_{tr} is <0.05.

Deposited-film flow. From the similarity solution, *Eq. 11*, $H(X)$ is plotted for several values of time *T* in Fig. 10. The smallest dimensionless value of *T*, $T = 200$, was chosen so that *H* does not exceed the critical value for closure. Also, in dimensional terms, this value is quite small, implying that we can apply this similarity solution to accurately predict the position of the leading edge of the bolus with time. Figure 10 shows that $H = h/r$ increases with distance for fixed *T*, but the dimensional film thickness *h* diminishes with *X*. Because surface-tension effects are being neglected, there is a sharp leading edge where *H* drops to 0. With time, the leading edge of the bolus advances, causing the film to thin. It takes ~6,000 time units for the leading edge to reach *generation 7*, where *H* is of the same order as H_M. In Fig. 11, the front location $\lambda(T)$ is plotted for several values of the product $W_b\Lambda$. It shows that initially the leading edge advances quite rapidly, but, as λ approaches the more distal airways, the rate of increase slows down as the liquid bolus is shared between an increasing number of airways. From *Eq. 11*, the dimensionless time taken for the front of the deposited film to move a distance λ by gravity is found by inverting the definition for $\lambda(T)$ in *Eq. 11*

$$T = \frac{1}{W_b^2\Lambda^2}\left[(1-\lambda)^{-1/2} - 1\right]^2 \qquad (17)$$

For example, the time required for the film front to reach *generation 7* in an adult, where $X = 0.8$, is $T \approx 1.5/(\Lambda W_b)^2$. For an adult lung, this corresponds to

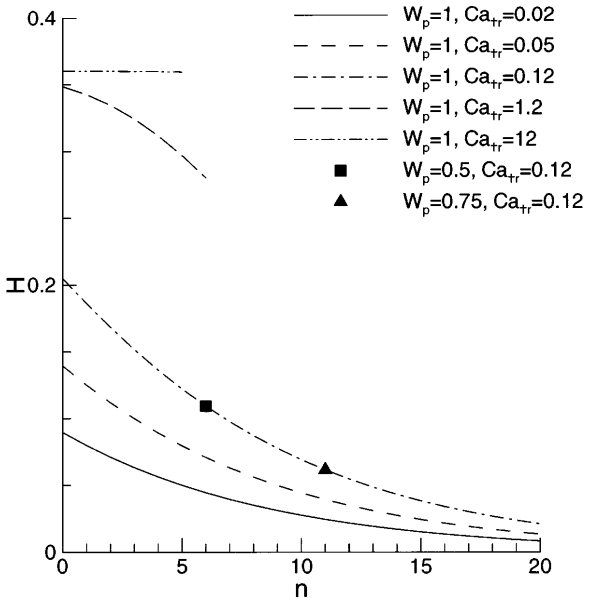

Fig. 9. Effect of Ca_{tr} on film thickness-to-airway radius ratio *H* vs. generation number *n*. Symbols denote where plug ruptures were for given W_p.

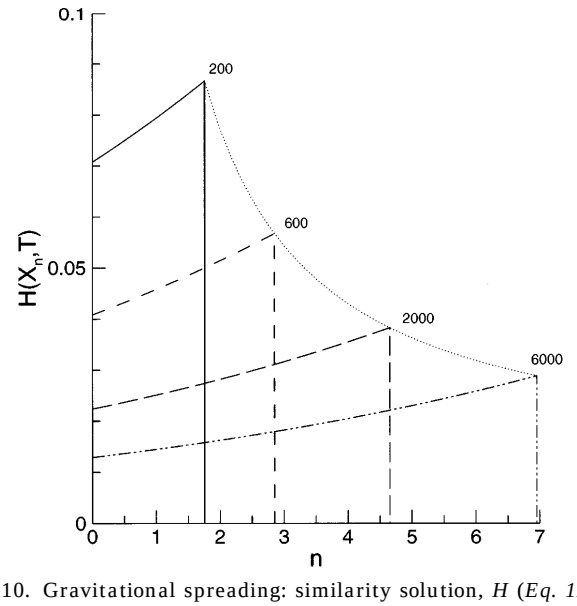

Fig. 10. Gravitational spreading: similarity solution, *H* (*Eq. 11*), is plotted against airway generation number *n* at times indicated. Dotted line shows height of bolus at its leading edge as a function of position. Parameter values are $W_p = 0.098$ and $\Lambda = 0.2$.

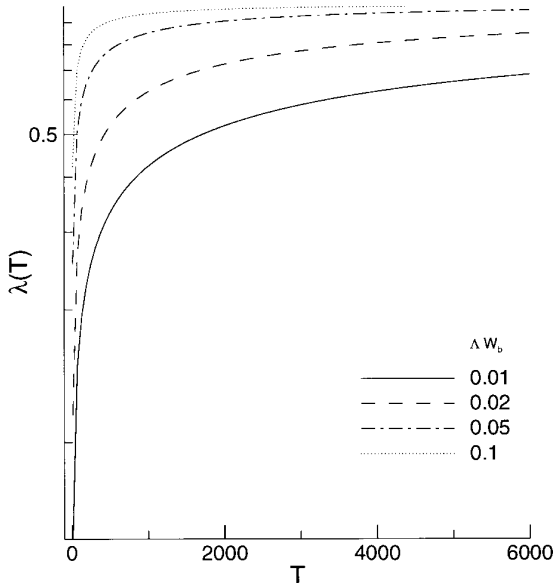

Fig. 11. Leading edge of bolus λ vs. time T for different values of ΛW_b. See *Glossary* for definitions.

$0.000833/(\Lambda W_b)^2$ s, and for a premature neonate the time taken is $0.0052/(\Lambda W_b)^2$ s, when using $\mu = 0.01$ g·cm^{-1}·s. Approximately the same values are obtained when a perfluorocarbon liquid such as Liquivent is used, since it has approximately the same kinematic viscosity as water ($\mu = 0.0184$ g·cm^{-1}·s; see Ref. 74), but the dimensional time can be considerably larger if Survanta is used, which is 60 times more viscous than water (F. F. Espinosa, personal communication).

For a liquid bolus with $V_b = 3$ cm^3, having the viscosity of water, the leading-edge film thickness falls beneath the critical film thickness of 50 μm (at which gravitational and Marangoni forces are of equal magnitude in the adult) after ~3 s (Liquivent) or 181 s (Survanta) at $X = 0.832$, very close to *generation 7*. [For larger V_b, the bolus travels quicker and deeper into the lung before reaching the critical height: for example, if $V_b = 1$ (or 5) cm^3, the critical height is reached at *generation 4* (or *9*) after 6.3 (or 2.02) s.]

Thereafter, fluid drains past this location, providing a continuous flux of material to the distal generations. By integrating the volume flux at *generation 7*, for example, with respect to time, it may be shown by using *Eq. 11* that the time taken for a fraction $(1 - \alpha)V_b$ of the fluid bolus to pass through *generation 7* is

$$T_\alpha = \frac{1}{(1 - X_7)W_b^2\Lambda^2\alpha^2} \qquad (18)$$

For $\alpha = 0.05$, 95% of the fluid drains past *generation 7* in time $T_\alpha = 2 \times 10^3/(W_b^2\Lambda^2)$. For an adult, by using the values of $W_b\Lambda$ shown in Fig. 11, the time taken for 95% of the bolus to reach *generation 7* ranges from 1.85 to 185 min, whereas for a neonate it ranges from 11.57 min to 19.29 h. With the parameter values used above, the leading edge of a bolus with $V_b = 3$ cm^3 reaches *generation 7* in 3 s (181 s for Survanta), and then 95% of the fluid volume drains past this location in the next 48 min (48 h for Survanta). We note that these transport times are linearly dependent on $1/g$, from the dimensional versions of *Eqs. 17* and *18*. Airways that, on the average, are not vertically oriented will have a smaller gravity component, and transit time will be lengthened accordingly in those regions.

Equations 10, *11*, *17*, and *18* can be applied past *generation 7* if a constant-surface-tension bolus of perfluorocarbon is used. For example, the leading edge of a 3-cm^3 liquid bolus reaches *generation 17* of an adult lung at $T = [(1 - X_{17})^{-1/2} - 1]^2$, or 54 s, and 95% of the initial bolus arrives after $T_\alpha \approx 400/[(1 - X_{17})W_b^2\Lambda^2]$, or ~8 h. This order of magnitude increase in time between *generations 7* and *17* is primarily due to the rapid increase in surface area with path length.

For a neonate, the initial surface-tension gradient is distributed over a length of only 3.75 cm, so the representative critical film thickness is 200 μm. Taking the infant tracheal radius to be 0.18 cm, this thickness represents ~11% of the tracheal radius. With a bolus volume $V_b = 0.5$ cm^3, for example, we find that the leading edge reaches *generation 7* in ~0.05 s, and 95% passes through *generation 7* in 64 min if Liquivent is used or in 2.94 s and 64 h, respectively, if Survanta is used. If such a large bolus volume is delivered at a single instant, the bolus fluid would occupy a substantial proportion of each airway, with the potential for temporarily occluding some airways. This could happen, for example, in liquid ventilation, where a bolus of fluorocarbon is forced along the trachea. However, if a liquid bolus is delivered slowly, a thin film forms on the airway walls. Under such conditions, gravitational effects would be dominated everywhere by surface-tension gradients, and our Marangoni-flow model would be appropriate.

Surface-layer transport. The following parameter values are chosen for the surfactant-spreading model derived in FORMULATION OF THE MODEL, *Surface-layer transport*. The bolus viscosity, and that of the liquid lining in the generations of interest, is taken to be that of water, so $\mu = 0.01$ g·cm^{-1}·s. The reference film thickness for an adult is chosen to be $h_7 = 20$ μm, which corresponds to 1% of the diameter of airway *generation 7*. The path length from trachea to alveoli in the adult is ~15 cm, so the path length from *generation 7* to the acinar region gives a length scale $L_M = 2.74$ cm. The computational domain is taken to be 11 generations, so the downstream boundary condition is imposed at *generation 18*, and we set the domain length $\hat{X}_a = 0.921$. The scale for the surface-tension difference driving the spreading is taken to be $S_7 = 50$ dyn/cm. The Marangoni time scale $T_M = \mu L_M^2/(S_7 h_7)$ is, therefore, $\sim T_M = 0.75$ s for an adult. For a neonate, where the bolus is delivered slowly so that the fluid lining remains thin, the same time scale applies. A key aim of our calculations is to determine how surface-area expansion, and the effects of preexisting surfactant, leads to transit and delivery times for exogenous surfactant that may be significantly in excess of T_M.

The effect of increasing preexisting surfactant concentration, Γ_A, is shown in Fig. 12 where all parameter

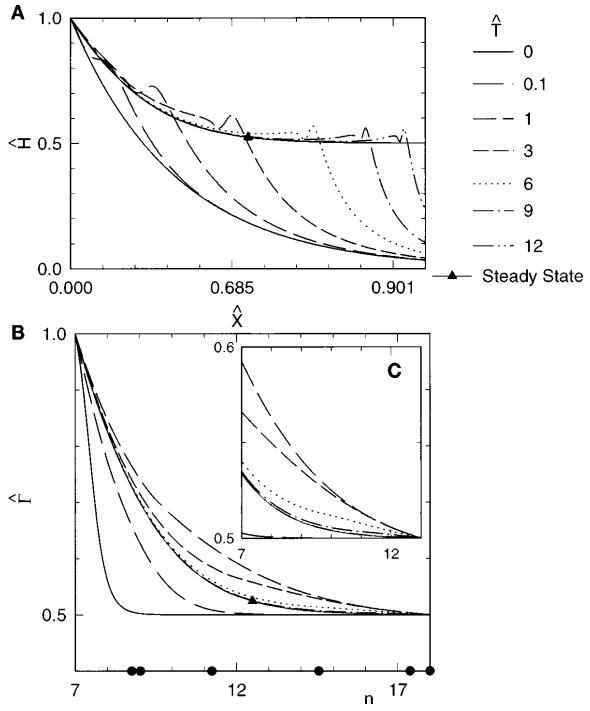

Fig. 12. $\hat{H}(\hat{X},\hat{T})$ (*A*) and $\hat{\Gamma}(\hat{X},\hat{T})$ (*B*, *C*) vs. $\hat{X}$ and n at $\hat{T} = 0$, 0.1, 1, 3, 6, 9, and 12, incorporating effects of surface-area expansion, with $\Gamma_A = 0.5$ and $\Delta = 0$. Solid curves with symbols show the ultimate steady state; ● in *B* show leading edge of exogenous surfactant distribution at times 0, 0.1, 1, 3, 6, and 6.95. See *Glossary* for definitions.

values are as in Fig. 5, except that $\Gamma_A = 0.5$ and the computations are carried out for a longer time until a steady-state solution is obtained. As predicted by Refs. 16, 28, and 42, the effect of increasing Γ_A is to force $\hat{\Gamma}$ and $\hat{H}$ to have smoother distributions near the disturbance's leading edge at early times [compare, for example, $\hat{\Gamma}(\hat{X},0.1)$ in Figs. 5*B* and 12*B*]. However, once the disturbance reaches the downstream end of the domain, the leading edge of $\hat{H}$ becomes steeper and the film thicker behind the leading edge. This is because surface-tension gradients are very small in the distal generations, and, therefore, a greater volume of fluid is entering these airways than is leaving. The film thickness at the downstream end, $\hat{H}(n = 18,\hat{T})$, increases with $\hat{T}$ until there is a balance of fluxes at $n = 7$ and $n = 18$. When this occurs, the liquid-lining thickness is approximately six times its initial value. However, airway closure is not likely to occur because it takes a very long time to reach steady state, and we are assuming that the liquid lining is initially very thin.

Because the effects of surface-area expansion cause the surface-tension gradient to be small at the distal end, other effects such as a pressure-gradient-driven flow due to the decrease in airway radius with distance from the trachea may become important. In Fig. 13, we have plotted $\hat{H}$ and $\hat{\Gamma}$ for $\Gamma_A = 0.5$ and $\Delta = 0.01$, obtained by solving *Eq. A1* numerically. Note that the preexisting surfactant is assumed to have an initially nonuniform distribution $\hat{\Gamma}_{eq}(\hat{X})$ (given by *Eq. A3*, and visible for $n > 9$ in Fig. 13, *B* and *C*) in which $\hat{\Gamma}$ increases slowly with respect to $\hat{X}$: this generates a weak, proximally directed shear stress at the free surface that opposes the shear stress generated by the curvature-driven flow, ensuring that the free surface is initially immobile. Once the exogenous surfactant starts to spread, the disturbances at the upstream end of the domain are very similar to those shown in Fig. 12, since the flow induced by surfactant gradients is much larger than the curvature-driven flow. Similarly, at the downstream end, where at first the surfactant concentration is relatively uniform, the distally directed flow causes preexisting surfactant to be swept toward $\hat{X} = \hat{X}_a$, so that $\hat{\Gamma}$ increases rapidly above the level $\hat{\Gamma}_{eq}(\hat{X}_a)$ for $0 < \hat{T} < 1$ (see Fig. 13*C*). However, as the surfactant-driven flow approaches equilibrium, it weakens relative to the curvature-driven flow, and $\hat{\Gamma}$ again falls beneath $\hat{\Gamma}_{eq}(\hat{X}_a)$ (e.g., $\hat{T} = 12$ in Fig. 13*C*), until ultimately a steady state is achieved. An important effect of the weak curvature-driven flow is to prevent the film thickness at the downstream end from becoming too big, reducing the likelihood of airway closure (Fig. 13*A*).

The leading edges of the exogenous surfactant distribution L_{ex} and of the surface-compression wave L_D are plotted vs. time in Fig. 14. As in Ref. 28, L_{ex} lags significantly behind L_D, since $\Gamma_A > 0$. However, whereas L_D is relatively insensitive to Γ_A and the effects of

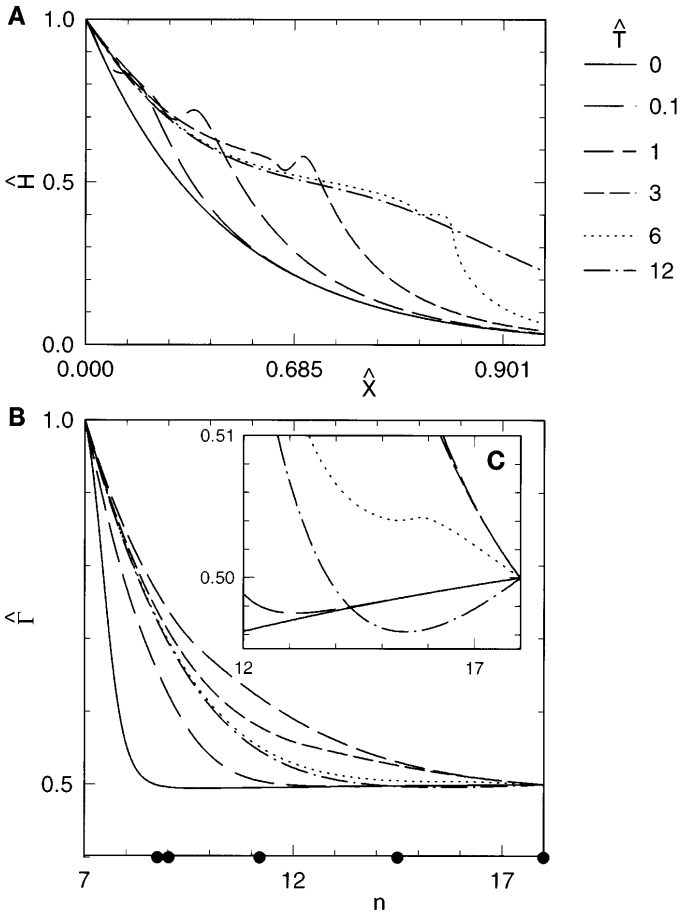

Fig. 13. $\hat{H}(\hat{X},\hat{T})$ (A) and $\hat{\Gamma}(\hat{X},\hat{T})$ (*B*, *C*) vs. $\hat{X}$ and n at $\hat{T} = 0$, 0.1, 1, 3, 6, and 12, including a weak curvature-driven flow, with $\Gamma_A = 0.5$ and $\Delta = 0.01$. ● in *B* show leading edge of the exogenous surfactant distribution at times 0, 0.1, 1, 3, 6, and 7.02. See *Glossary* for definitions.

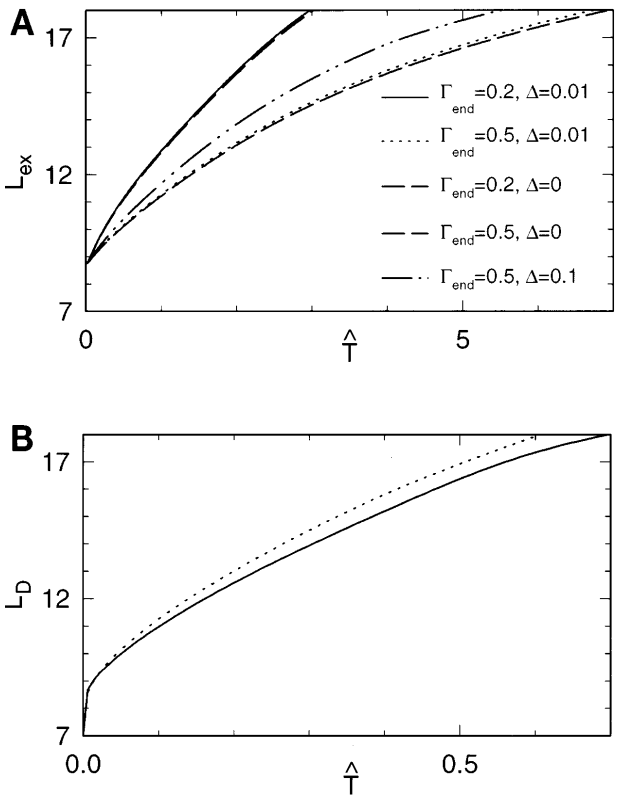

Fig. 14. *A*: L_{ex} vs. $\hat{T}$ for $\Gamma_A = 0.2$ and 0.5 and $\Delta = 0$, 0.01, and 0.1. *B*: L_D vs. $\hat{T}$ for $\Gamma_A = 0.2$, $\Delta = 0.01$ and $\Gamma_A = 0.5$, $\Delta = 0.01$. See *Glossary* for definitions.

surface-area expansion, reaching *generation 18* at $\hat{T} \approx 0.55$, or 0.41 s (Fig. 14*B*), this is not so for L_{ex}: for $\Gamma_A = 0.2$, it takes approximately three time units, or 2.25 s, for exogenous surfactant to reach the downstream end, an order of magnitude longer than if there were no surface-area expansion. The rate of advance of L_{ex} falls in the distal generations due to the effects of surface-area expansion and the increased flow resistance due to a decrease in liquid-lining thickness. An increase in Γ_A to 0.5 causes the arrival time of exogenous surfactant to more than double. The effect of curvature-driven flow on the time taken for exogenous surfactant to reach the respiratory bronchioles is not significant (Fig. 14*A*). It causes exogenous surfactant to reach *generation 18* marginally later than the $\Delta = 0$ case and has its biggest impact in the distal generations where surface-tension gradients are weakest.

Surface-layer transit time in the steady state. The effect of the initial preexisting surfactant concentration Γ_A on surface-area expansion can be further investigated by determining the transit time, $\hat{T}_s$, for exogenous surfactant to cross the whole domain once steady state is achieved (neglecting curvature-driven flow). $\hat{T}_s$ is computed from the equation that governs the Lagrangian motion of a particle on the air-liquid interface (28)

$$\frac{d\hat{X}}{d\hat{T}} = \hat{U}_s(\hat{X}, \hat{T}) = -\hat{H}\hat{\Gamma}_{\hat{X}} \tag{19}$$

where $\hat{U}_s(\hat{X},\hat{T})$ is the surface velocity (assuming for simplicity that $\Delta = 0$). At steady state, with the boundary conditions used above, $\hat{H} = \hat{\Gamma}$. Hence

$$\hat{T}_s = -\int_0^{\hat{X}_a} \frac{d\hat{X}}{\hat{\Gamma}\hat{\Gamma}_{\hat{X}}} \tag{20}$$

In the absence of surface-area expansion, the right-hand side of *Eq. 20* can be integrated analytically, using *Eq. 12*, to yield

$$\hat{T}_s = \frac{9}{4}\frac{1 - [1 - (1 - \Gamma_A^3)\hat{X}_a]^{4/3}}{(1 - \Gamma_A^3)^2} \tag{21}$$

Figure 15 shows that in this case $\hat{T}_s$ is only very weakly dependent on Γ_A for $0 < \Gamma_A \leq 0.5$ but increases by a factor of approximately five as Γ_A is increased from 0.1 to 0.9; the transit time becomes infinite as $\Gamma_A \rightarrow 1$. The dependence of $\hat{T}_s$ on Γ_A is influenced by the choice of boundary conditions: Jensen et al. (44), who used no-flux conditions on $\hat{\Gamma}$ and $\hat{H}$ at $\hat{X} = 0$ rather than assuming a steady source of exogenous surfactant there, so that their flow was always unsteady, found a much stronger dependence of $\hat{T}_s$ on Γ_A. However, when the effects of surface-area expansion are included in *Eq. 19*, $\hat{T}_s$ increases by more than a factor of 10 as Γ_A is increased from 0.01 to 0.95 (Fig. 15).

Dose delivery times: steady-state alveolar surface concentration. After the initial transients have decayed (within a few seconds of the initial delivery of the first surfactant dose), the steady-state flow in *generations 7–18* delivers a steady flux of surfactant to the alveolar space. This (nondimensional) flux, $-B\hat{\Gamma}\hat{H}\hat{\Gamma}_{\hat{X}}$, evaluated at $\hat{X} = \hat{X}_a$, where $\hat{\Gamma}$ and $\hat{H}$ are given by *Eq. 13*, is

$$Q_A = \frac{1 - \Gamma_A^3}{1 - (1 - \hat{X}_a)^3} \tag{22}$$

where Γ_A is the surface concentration of surfactant in the alveoli, which we treat as a well-mixed compart-

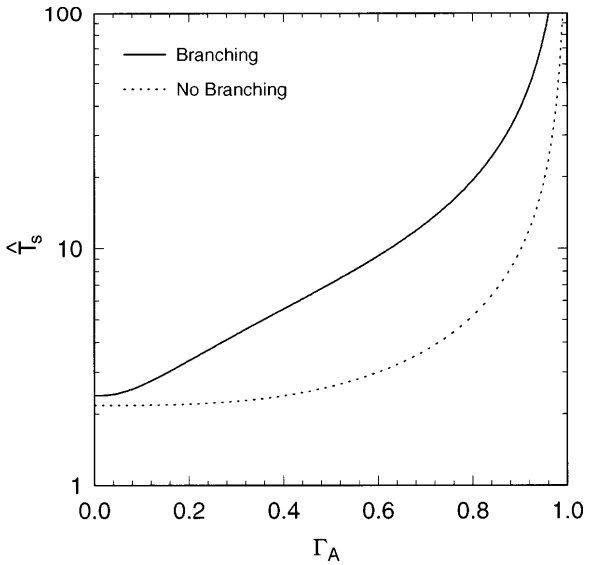

Fig. 15. Transit time ($\hat{T}_s$) for exogenous surfactant to cross domain at steady state as a function of Γ_A. Solid curve includes surface-area expansion effects, and dashed curve does not.

ment. We assume that the alveolar compartment comprises the entire transport regime distal to *generation 18*.

An estimate for the delivery time of the entire exogenous surfactant bolus can be made by using *Eq. 22*. Typical neonatal dose sizes are 100 mg/kg, given in two half-doses, 12 h apart (14). Therefore, an infant weighing 500 g receives two doses of 25 mg. So we take $m_{dose} = 25 \times 10^{-3}$ g. Adult dose sizes are also taken to be 100 mg/kg (13, 39, 69). This corresponds to an $m_{dose} =$ 3.5 g for a 70-kg adult. We take the micelle concentration to be the reference concentration at *generation 7* in an adult, so $\gamma_7 = 2 \times 10^{14}$ molecules/cm^2 (66). Because dipalmitoylphosphatidylcholine has molecular weight of 734 and $N_A = 6.02 \times 10^{23}$, $\gamma_7 = 2.44 \times 10^{-7}$ g/cm^2. For an infant, $L_M = 3.75$ cm, $b_7 = 1.13$ cm, so $\gamma_7 L_M b_7 = 1.03 \times 10^{-6}$ g, and $T_M = 0.75$ s (where this time scale is that defined for surfactant-driven flow in FORMULATION OF THE MODEL, *Deposited-film flow*). Thus the scale of the exogenous surfactant flux is $q_7 = \gamma_7 L_M b_7 / T_M = 1.37 \times 10^{-6}$ g/s approximately, which is an upper bound on the actual flux. We can therefore estimate the time for one dose to be delivered, assuming the conditions are steady state. Dividing the mass delivered by the mass flux (with $q_A = q_7$) yields a delivery time = 25×10^{-3} g/(1.37×10^{-6} g/s) = ~5 h.

Dose delivery times: quasi-steady alveolar surface concentration. The exogenous surfactant that arrives at the alveolar compartment is not taken up immediately. It accumulates and is removed by processes with a long half-life, i.e., 5–15 h. This time scale, used to define τ in *Eq. 15*, is long compared with the time required to reach steady state in the delivery process. Therefore, we may treat the alveolar concentration, at *generation 18* in our model, as time dependent on the slow time scale and suppose the flux Q_A depends only on Γ_A when *Eq. 22* is used. Then, using *Eq. 22*, *Eq. 15* becomes

$$\frac{d\Gamma_A}{d\tau} = \hat{F}(1 - \Gamma_A^3) - \Gamma_A + P_A \qquad (23)$$

where $\hat{F} = F/[1 - (1 - \hat{X}_a)^3]$. If $\hat{F} = 0$, so that there is no supply of exogenous surfactant, the alveolar surfactant concentration has an equilibrium value in which natural supply and uptake balance, i.e., $\Gamma_A = P_A$. This value will be smaller than the level of exogenous concentrations, so that $0 < P_A < 1$. We now consider the evolution of the system for $\hat{F} > 0$.

Suppose that at $\tau = 0$, $\Gamma_A = P_A$, and $\hat{F} > 0$. Then Γ_A will rise with time, approaching a new equilibrium value $\Gamma_A = \Gamma_{eq}$, say, where $\Gamma_{eq} = \Gamma_{eq}(\hat{F}, P_e)$ satisfies

$$\hat{F}(1 - \Gamma_{eq}^3) - \Gamma_{eq} + P_A = 0 \qquad (24)$$

Figure 16 shows how Γ_{eq} depends on $\hat{F}$ and P_A. As $\hat{F}$ increases for fixed P_A, Γ_{eq} rises from P_A (when $\hat{F} = 0$) toward 1. For small $\hat{F}$, the delivered flux is weak, so that alveolar concentrations are close to their undisturbed values. For large $\hat{F}$, the rate of uptake is relatively weak compared with the flux of exogenous material, so that over sufficiently long times the alveolar surfactant concentration can rise close to the level of the exogenous surfactant supply. As P_A increases, the equilibrium levels all rise: an increase in natural surfactant production may be stimulated by the delivery of exogenous material. Figure 17 shows how the alveolar concentration $\Gamma_A(\tau)$ rises slowly to its equilibrium value, driven by the flux of exogenous material. This equilibrium is reached in principle after an infinite time. In practice, however, the dose delivered to *generation 7* is of finite size, so that after a finite time the source dries up. We must therefore compute the time taken for the full dose to be delivered to the alveoli.

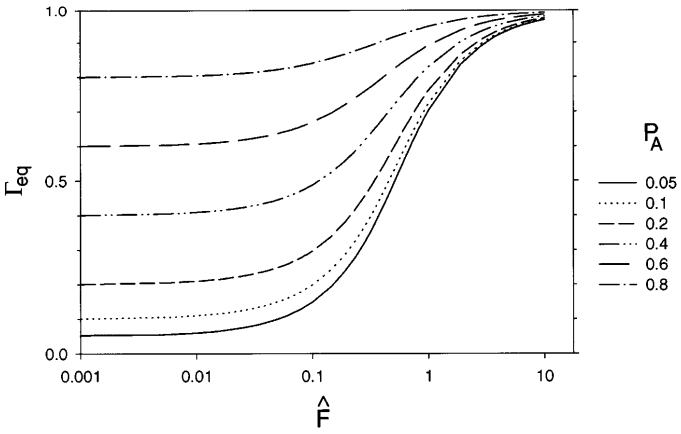

Fig. 16. Steady-state alveolar surfactant concentration Γ_{eq} vs. rate of supply of exogenous surfactant $\hat{F}$ for several rates of supply of endogenous surfactant, P_A.

Therefore, we compute the integral of the flux of surfactant delivered to the alveoli. The mass of exogenous surfactant delivered in time τ_D is

$$m(t_D) = \int_0^{t_D} q_s \, dt \qquad (25)$$

In terms of the nondimensional variables used in *Eq. 23*

$$M(\tau_D) = \frac{m(t_D)}{A_A \gamma_7} = \hat{F} \int_0^{\tau_D} (1 - \Gamma_A^3) d\tau \qquad (26)$$

where $\tau_D = t_D K$. Using parameter values given in *Dose delivery times: steady-state alveolar surface concentration*, with $A_A = 3.6$ m^2 for an infant and 90 m^2 for an adult, delivery times for $M = m_{dose}/(A_A \gamma_7) = 3$ (for an infant) and $M = 16$ (for an adult), computed by using *Eqs. 23* and *26*, are plotted for various values of P_A and $\hat{F}$ in Fig. 18. Γ_A will rise from P_A at $\tau = 0$ toward its equilibrium value $\Gamma_{eq}(P_A, \hat{F}) < 1$ as τ increases, until a dose M is delivered at $\tau = \tau_D$. Figure 18 shows that τ_D decreases if the rate of delivery of exogenous surfactant is increased ($\hat{F}$) or if the supply of endogenous surfactant is increased. When the dose is fully used up, the alveolar surfactant concentration will fall again to its equilibrium value P_A, which may now be larger if P_A has increased as Γ_A increased. For a neonate, $2.5 \leq \tau_D \leq 12$, given $2.6 \leq \hat{F} \leq 7.2$. Therefore, for a rate constant $K = 0.138$/h, the total delivery time ranges from 18 to 87 h. Usually a second dose is delivered 12–24 h after the first dose. This correlates well with our findings, provided P_A is sufficiently large. For an adult, given $K = 0.138$/h, $\hat{F} \approx 1$ and, from Fig. 18*B*, $25 \leq \tau_D \leq 104$. This corresponds to delivery times ranging from 1 wk to

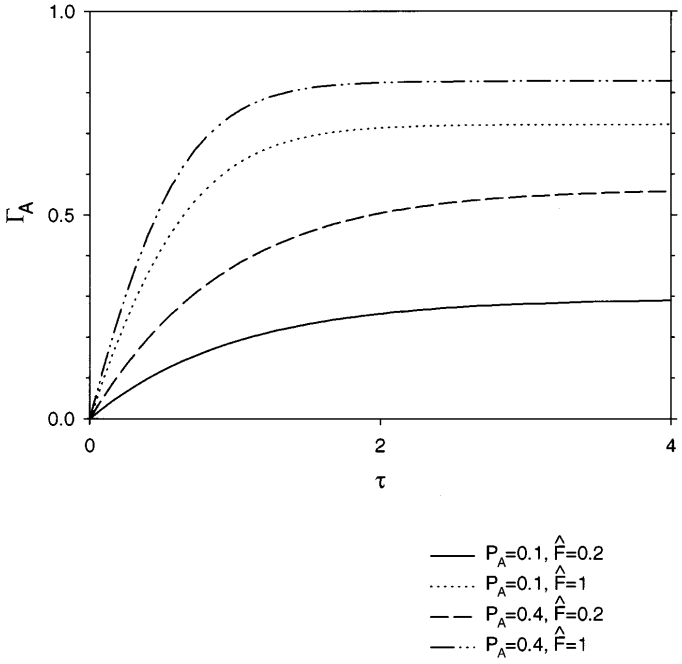

Fig. 17. Alveolar equilibrium surfactant concentration $\Gamma_A(\tau)$ vs. τ for several values of P_A and $\hat{F}$.

1 mo and may provide an explanation for the lack of long-term success of SRT with ARDS patients (36).

DISCUSSION

This model, although a greatly simplified picture of the true spreading process, captures some important elements of the transport of a bolus of exogenous surfactant to the lung periphery. A liquid plug of surfactant is initially driven by the inspiratory airflow in the upper airways. It loses volume as it propagates to the distal airways, leaving behind a deposited liquid layer that coats the airways. A simple theory shows that rupture of the plug, when its volume decreases to zero, depends on the magnitude of the airflow rate and the ratio of initial plug volume to tracheal volume. Our model indicates that plugs with initial volumes <1 cm^3, approximately, will rupture in the first seven generations, even at high flow rates. Larger plugs may never rupture in one breath but they may stop once they reach a collapsed region of the lung. The thickness of the deposited liquid lining may become sufficiently thick that the liquid coating will start to drain under the effect of gravity.

The effects of gravity are dominant in the upper airways of the adult lung: a simple similarity solution, *Eq. 11*, suggests that, for typical bolus volumes, gravity carries the surfactant to *generations 5–9* in a few seconds (Fig. 10) and provides thereafter a continuous flux of surfactant to the distal portions of the lung for many minutes. The bolus fluid, which is distributed around the airway walls, becomes so thin near these generations because of surface-area expansion effects that gravitational forces weaken, relative to surface-tension gradients, so that Marangoni flows drive the surfactant deeper into the lung. Distally directed curvature-driven flow was shown to have only a very weak effect on transit times (Fig. 13), although it had a much more pronounced effect on film distributions. Despite the significant surface-area expansion that the monolayer experiences as it advances further, the model predicts that surface-tension reduction is initially experienced at the terminal bronchioles very rapidly, within ~0.5 s (Fig. 14*B*) of the bolus reaching *generation 7*. This is so because the advancing exogenous surfactant compresses preexisting surfactant: the higher the concentration of preexisting material, the quicker an initial surface-tension reduction is experienced. Hence, surface compression of a preexisting surfactant layer, possibly occurring well before the exogenous surfactant actually arrives at a target airway or alveolus, may be a therapeutically valuable effect.

We model surfactant uptake by alveolar type II cells (7) as a sink by fixing the surfactant concentration to be constant at *generation 18*. Even so, the level of preexisting surfactant, Γ_A, remains an important parameter. Exogenous surfactant was predicted to arrive at *generation 18* within ~2.25 s of leaving *generation 7* (Fig. 14*A*) when $\Gamma_A = 0.2$; this transit time rose to ~4.5 s with $\Gamma_A = 0.5$. A steady balance of fluxes between material provided by gravity-driven flow at *generation 7* and being taken up at *generation 18* was established in most cases within ~10 s; the time taken for exogenous surfactant to be advected to the periphery from *generation 7* by

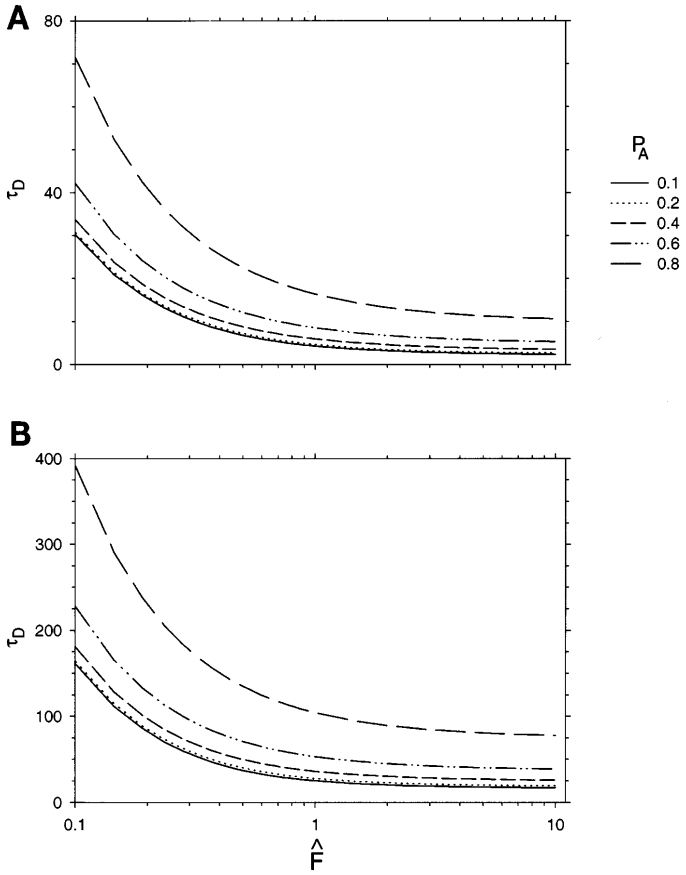

Fig. 18. Delivery time τ_D vs. $\hat{F}$ for different p_A. *A*: $M = 3$ (infant); *B*: $M = 16$ (adult). See *Glossary* for definitions.

this steady flow is strongly dependent on the level of preexisting surfactant, ranging from a few seconds for $\Gamma_A \rightarrow 0$ to a few minutes as Γ_A approaches its tracheal concentration ($\Gamma_A \rightarrow 1$, Fig. 15). This is consistent with the fact that spreading rates are reduced as the surfactant level builds up in the lung (28) and correlates with observations that neonatal patients may respond to the first intratracheal bolus of surfactant, but that subsequent instillations, e.g., beyond two, are not as effective (54). They may follow the same opened pathways as the first dose (73) and, therefore, may not be going to untreated regions of the lung.

The surfactant concentration at the distal end of the Marangoni flow regime is held constant because the time scale for alveolar surfactant uptake is much longer than the time scale for the Marangoni flow. The alveolar surfactant concentration actually increases slowly as a result of the flux of exogenous surfactant generated by the Marangoni flow. A surfactant kinetics model is employed by using available data for the time constant of uptake. The quasi-steady-state balance of Marangoni delivery with alveolar uptake determines the delivery time of a given dose of surfactant, with the alveolar surfactant production rate as a parameter. For neonates, it takes ~24 h for a 2.5-cm^3 bolus to be delivered. Delivery times are reduced by increasing either the rate of delivery of exogenous surfactant or the alveolar surfactant production rate with respect to the rate constant for surfactant uptake.

To apply the thin-film model to the infant lung, it was necessary to assume that the surfactant bolus was delivered to the trachea sufficiently slowly that the bolus fluid always formed a thin layer around the lung airways. If this is the case, then the liquid layer is everywhere so thin that surface-tension gradients dominate over gravitational forces. To model the morphometry of the immature infant lung, we made the crude assumption that it can be represented by that portion of an adult lung distal to a single airway at *generation 7*. The calculations appropriate for the adult lung then carry over directly to this case: surface-tension reduction at the periphery is experienced within ~0.5 s; fresh material reaches the alveoli within 3–6 s. These times will obviously be reduced if a larger bolus is introduced rapidly into the trachea, because gravitational spreading will enhance the rate of delivery, but the larger volume of fluid may possibly occlude the airways temporarily and cause choking.

There are many aspects of surfactant transport that have been neglected, which should be considered in future models. The lining fluid has been taken to be a Newtonian fluid with viscosity similar to that of water, which is unreasonable in the upper airways. In addition, we have omitted clearance by ciliary transport. The surfactant has been supposed to have a linear equation of state (i.e., constant surface activity), whereas, in practice, the relationship between surface tension and surfactant concentration is typically nonlinear, particularly at high concentrations. We have assumed that the exogenous and preexisting surfactants have the same surface activity. It is, instead, possible that there could be physicochemical interactions between the chemically distinct exogenous and preexisting materials, which would contribute to these nonlinearities and, hence, influence spreading rates.

The model of the lung is necessarily simple, to make calculations tractable. The dichotomous branching model used to develop a formula for the airway circumference function $B(X)$ (*Eq. 3*) is highly idealized, particularly since asymmetries in the lung are neglected; there is a need for more reliable functions to be developed by using realistic morphometric data, especially for developing neonatal lungs. A particularly important aspect of SRT, which this model is presently unable to address, is inhomogeneous spreading, which arises both in gravity-driven and Marangoni-driven spreading. In the former case, the surfactant bolus will drain rapidly vertically downward, and, even if the patient is rolled around it, it is likely that the spreading may be nonuniform; there is scope for improving the model for gravity-driven flow (see FORMULATION OF THE MODEL, *Surface layer transport*) to take this and other factors into account. In the latter case, a portion of the lung that is well ventilated will have patent airways down which surfactant can progress relatively easily, whereas the monolayer is unlikely to advance as quickly into atelectatic regions. The mechanism by which airways reopen, and the role played by surfactants in this process, is being investigated elsewhere (23). The effects of inhomogeneity are felt particularly strongly when the lung is being ventilated, since the patent airways tend to overdistend.

The interaction between surfactant transport and ventilation, either spontaneous or forced, deserves attention: the unsteady expansion and contraction of the airway walls, the importance of dynamic surface tension, and the role of air shear stresses should be investigated. At smaller scales, inhomogeneities in the advance of the monolayer are likely to develop in the neighborhood of an airway bifurcation. The nonuniform curvature of the airway wall may cause the airway liquid lining to assume a configuration in which it is of nonuniform thickness (41) (by draining away from the vertex of a bifurcation, for example). An advancing monolayer will travel quicker over thicker fluid layers, so that by neglecting details of airway structure we may be neglecting important features of the spreading process.

Finally, with use of our results, it is interesting to consider clinical delivery strategies. Making the instilled volume larger enhances rapid gravity-driven spreading but risks both ventilatory obstruction and strongly inhomogeneous delivery. Also, the larger the plug the further it penetrates into the lung before rupturing. For delivery of liquids that may carry drugs or genetic material intended for airway walls, the smaller plug will rupture before reaching the alveoli, so that the contents coat the targeted airways. Surfactant transport to the periphery by the Marangoni mechanism is controlled predominantly by the level of preexisting surfactant: Fig. 15 shows that for $0.1 < \Gamma_A < 0.7$ (approximately) the dependence of spreading rates on

Γ_A is greater if the effects of surface-area expansion are included in the model than if they are absent. Rapid spreading of fresh exogenous material occurs if Γ_A is low; once Γ_A increases beyond, say, 0.9 (as it might after repeated small doses), there may be no significant gain in delivering additional exogenous surfactant. However, the film deformations arising in this case are potentially severe: although those in Fig. 5, for example, are not particularly dramatic, under different boundary conditions (e.g., Ref. 43), we found that severe thickening or thinning of the film can occur, increasing the risks of either airway closure or rupture of the lining film. (In some cases, it was even possible to cause the film to overturn.) These findings support the study of Alvarez et al. (2), who found that four fractional surfactant doses given to rats with damaged lungs gave no enhancement over the same total dose delivered as a single bolus. Although combining the bolus and aerosol techniques may be effective (28), the bolus to open airways and the aerosol to bypass any slow-moving Marangoni regions, there remains the difficulty that aerosolized material may go where it is least needed, i.e., to the best ventilated portions of the lungs.

APPENDIX

Evolution Equations for Surface-Area Expansion Models

We suppose that as the surfactant advances because of surface-tension forces, its concentration and the film thickness of the airways it traverses are dependent only on distance along the pulmonary tree and on time. We are not considering variations in film thickness or surfactant concentration among airways of the same generation, so no allowance is made for inhomogeneous spreading. The liquid lining is assumed to be sufficiently thin everywhere so that it can be treated as locally planar. By considering conservation of fluid mass and conservation of surfactant, we obtain the dimensionless governing equations for the film thickness, $\hat{H}(\hat{X},\hat{T}) = h(x,t)/h_7$, and the surfactant concentration, $\hat{\Gamma}(\hat{X},\hat{T}) = \gamma(x,t)/\gamma_7$, which are derived in a manner similar to our previous studies (22, 28, 42, 44)

$$\hat{H}_{\hat{T}} + \frac{1}{\hat{B}}(\hat{B}Q)_{\hat{X}} = 0, \qquad Q = -\left(\frac{1}{2}\hat{H}^2\hat{\Gamma}_{\hat{X}} - \frac{\Delta}{3}\hat{H}^3\frac{\hat{R}_{\hat{X}}}{\hat{R}^2}\right)$$

$$\hat{\Gamma}_{\hat{T}} + \frac{1}{\hat{B}}(\hat{B}q)_{\hat{X}} = 0, \qquad q = -\left(\hat{H}\hat{\Gamma}\hat{\Gamma}_{\hat{X}} - \frac{\Delta}{2}\hat{H}^2\hat{\Gamma}\frac{\hat{R}_{\hat{X}}}{\hat{R}^2}\right) \tag{A1}$$

where Q and q are the fluxes of fluid and surfactant, respectively. The first term in the expression for the fluxes is due to Marangoni effects, whereas the second is due to the axial variation in airway radius. The dimensionless independent variables are the axial distance, $\hat{X} = x/L_M$, and time, $\hat{T} = t/T_M$, where $T_M = L_M/U_M$. h_7 is the reference film thickness at *generation 7* in the adult, and L_M is the length of the Marangoni region, $L_M = x_{18} - x_7$. U_M is the characteristic Marangoni velocity scale for the interval $x_{18} - x_7$. It is defined by $U_M = S_7 h_7/\mu L_M$, where $S_7 = \theta\Gamma_7$. The surfactant activity θ represents the surface-tension-reducing capacity of the monolayer and is taken to be constant, which is equivalent to assuming a linear equation of state for the surface tension-surface concentration relationship. Therefore, U_M represents a balance of surface-tension gradient forces to viscous shear resistance. Then $T_M = \mu L_M^2/S_7 h_7$ represents the time required for Marangoni convection over the distance L_M. The dimensionless perimeter function is $\hat{B}(\hat{X}) = \beta B(\hat{X})$, where $\beta = b_0/\pi d_7$ for a neonate and $\beta = b_0/b_7$ for an adult. Thus the relevant perimeter scaling for the adult is b_7, the total perimeter of all airways at *generation 7*, whereas the appropriate scale for the neonate is its tracheal perimeter, taken as the equivalent of a single adult *generation 7* airway, πd_7. Here, $\Delta = (\sigma_m/S_7)(h_7/r_7)$, where σ_m is the mean interfacial surface tension in the computational region. This approximation is accurate for the mean ratio $h_7/r_7 << 1$ and has an error of magnitude $(h_7/r_7)^2$.

The boundary conditions on the governing *Eq. A1* are as follows. The surfactant concentration is fixed at the proximal boundary of the Marangoni domain, $\hat{X} = 0$, to be unity and, at the distal end of the domain, $\hat{X} = \hat{X}_a$ (*generation 18*) to be the alveolar value, Γ_A, that is

$$\hat{\Gamma}(\hat{X} = 0, \hat{T}) = 1, \qquad \hat{\Gamma}(\hat{X} = \hat{X}_a, \hat{T}) = \Gamma_A < 1 \tag{A2}$$

Hence, a continuous surfactant supply is available as input to the Marangoni domain as the bolus drains under gravity from proximal generations (this assumption is justified in RESULTS, *Deposited-film flow*). We take the alveolar surfactant concentration to be constant, $\Gamma_A = 0.2$ or 0.5. The latter condition is motivated by the observation (7) that exogenous surfactant is taken up in alveolar type II cells, so that a continual flux of surfactant in the distal direction can be supported.

Steady-state solutions to *Eq. A1* may be derived by setting the time derivatives to zero. An interesting subset of such solutions is an equilibrium solution that balances Marangoni and capillarity effects, i.e., no surfactant flux. This state could represent the preexisting surfactant distribution before any new surfactant is added to the system. The equilibrium solution is obtained by setting $q = 0$ and $Q =$ constant in *Eq. A1*, and is chosen to satisfy the distal boundary condition for $\hat{\Gamma}$ and the proximal boundary condition for $\hat{H}$. The result is

$$\hat{H}_{eq}(\hat{X}) = (1 - \hat{X})^{4/3},$$
$$\hat{\Gamma}_{eq}(\hat{X}) = \Gamma_A + \frac{3\Delta}{2}[(1 - \hat{X}_a)^{1/3} - (1 - \hat{X})^{1/3}] \tag{A3}$$

We may now employ these equilibrium solutions in posing the initial conditions for the unsteady problem. Consider an additional amount of surfactant added to the equilibrium distribution that represents the exogenous material. Keeping the same liquid-layer thickness distribution, we have the initial conditions

$$\hat{H}(\hat{X}, \hat{T} = 0) = \hat{H}_{eq}(\hat{X})$$
$$\hat{\Gamma}(\hat{X}, \hat{T} = 0) = \hat{\Gamma}_{eq}(\hat{X}) + \left[\frac{1 - \hat{\Gamma}_{eq}(0)}{2}\right]\left[1 + \tanh\left(\frac{\xi_2 - \hat{X}}{\xi_1}\right)\right] \tag{A4}$$

where ξ_2 and ξ_1 are constants chosen to make the initial surfactant distribution match the boundary conditions.

These equations (*A1*, *A2*, and *A4*) are solved numerically by using the method of lines. We assume that the liquid lining is Newtonian with uniform viscosity, although the model can readily be modified to allow for viscosity variation. The terms involving Δ are generally very small compared with the Marangoni terms. The two mechanisms may become comparable only in the most distal airways where $\hat{R}$ becomes very small. For the case of a uniform tube, $\hat{B} = 1$, the initial conditions are given by *Eq. A4* with $\hat{H}_{eq}(\hat{X}) = 1$ and $\hat{\Gamma}_{eq}(\hat{X}) = \Gamma_A$.

This study was supported by North Atlantic Treaty Organization Grants CRG-930189 and CRG-950725; by the Whitaker Foundation; by National Science Foundation (NSF) Grant CTS-9412523; by National Heart, Lung, and Blood Institute Grant HL-41126; and by NSF Experimental Program to Stimulate Competitive Research in Alabama.

Present address of J. B. Grotberg: Biomedical Engineering, Univ. of Michigan, 3304 G.G. Brown, 2350 Hayward, Ann Arbor, MI 48109.

Address for reprint requests: D. Halpern, Dept. of Mathematics, Univ. of Alabama, Tuscaloosa, AL 35487.

Received 24 February 1997; accepted in final form 19 March 1998.

REFERENCES

1. **Acheson, D. J.** *Elementary Fluid Mechanics*. London: Oxford Univ. Press, 1990.
2. **Alvarez, F. J., L. F. Alfonso, E. Gastiasoro, J. Lopez-Heredia, A. Arnaiz, and A. Valls-i-Soler.** The effects of multiple small doses of exogenous surfactant on experimental respiratory failure induced by lung lavage in rats. *Acta Anaesthesiol. Scand*. 39: 970–974, 1995.
3. **Anzueto, A., R. P. Baughman, K. K. Guntupalli, J. G. Weg, H. P. Wiedemann, A. A. Raventos, F. Lemaire, W. Long, D. S. Zaccardelli, and E. N. Pattishall.** Aerosolized surfactant in adults with sepsis-induced acute respiratory distress syndrome. Exosurf Acute Respiratory Distress Syndrome Sepsis Study Group. *N. Engl. J. Med*. 334: 1417–1421, 1996.
4. **Bertling, W. M., M. Gareis, V. Paspaleeva, A. Zimmer, J. Kreuter, E. Nurnberg, and P. Harrer.** Use of liposomes, viral capsids, and nanoparticles as DNA carriers. *Biotechnol. Appl. Biochem*. 13: 390–405, 1991.
5. **Borgas, M. S., and J. B. Grotberg.** Monolayer flow on a thin film. *J. Fluid Mech*. 193: 151–170, 1988.
6. **Bretherton, F. P.** The motion of long bubbles in tubes. *J. Fluid Mech*. 10: 166–188, 1961.
7. **Chinoy, M., A. Fisher, and H. Shuman.** Confocal imaging of time-dependent internalization and localization of NBD-PC in intact rat lungs. *Am. J. Physiol*. 266 (*Lung Cell. Mol. Physiol*. 10): L713–L721, 1994.
8. **Colledge, W.** Cystic fibrosis gene therapy. *Curr. Opin. Genet. Dev*. 4: 466–471, 1994.
9. **Corbet, A., R. Bucciarelli, S. Goldman, M. Mammel, D. Wold, and W. Long.** Decreased mortality rate among small premature infants treated at birth with a single dose of synthetic surfactant: a multicenter controlled trial. *J. Pediatr*. 118: 277–284, 1991.
10. **Crystal, R.** Gene therapy strategies for pulmonary disease. *Am. J. Med*. 92: 44S–52S, 1992.
11. **Davis, J. M., G. A. Russ, L. Metlay, B. Dickerson, and B. S. Greenspan.** Short-term distribution kinetics of intratracheally administered exogenous lung surfactant. *Pediatr. Res*. 31: 445–450, 1992.
12. **Davis, S. H., A.-K. Liu, and G. R. Sealy.** Motion driven by surface-tension gradients in a tube lining. *J. Fluid Mech*. 62: 737–752, 1974.
13. **Enhorning, G.** Surfactant replacement in adult respiratory distress syndrome (Editorial). *Am. Rev. Respir. Dis*. 140: 281–283, 1989.
14. **Enhorning, G. E., A. Shennan, F. Possmayer, M. Dunn, C. P. Chen, and J. Milligan.** Prevention of neonatal respiratory distress syndromes by tracheal instillation of surfactant: a randomized clinical trial. *Pediatrics* 76: 145–153, 1985.
15. **Espinosa, F. F., and R. D. Kamm.** Delivery of pulmonary surfactant by tracheal instillation. *Ann. Biomed. Eng*. 24: S1–S11, 1996.
16. **Espinosa, F. F., A. H. Shapiro, J. J. Fredberg, and R. D. Kamm.** Spreading of exogenous surfactant in an airway. *J. Appl. Physiol*. 75: 2028–2039, 1993.
17. **Everett, D. H., and J. M. Haynes.** Model studies of capillary condensation 1. Cylindrical pore model with zero contact angle. *J. Colloid Interface Sci*. 38: 125–137, 1972.
18. **Feldbaum, D. M., D. Wormuth, G. F. Nieman, M. Paskanik, W. R. Clark, and T. S. Hakim.** Exosurf treatment following wood smoke inhalation. *Burns* 19: 396–400, 1993.
19. **Fisher, A., C. Dodia, and A. Chander.** Alveolar uptake of lipid and protein components of surfactant. *Am. J. Physiol*. 261 (*Lung Cell Mol. Physiol*. 5): L334–L340, 1991.
20. **Fuhrman, B. P., P. R. Paczan, and M. DeFrancisis.** Perfluorocarbon-associated gas exchange. *Crit. Care Med*. 19: 712–722, 1991.
21. **Gaver, D. P., and J. B. Grotberg.** Droplet spreading on a thin viscous film. *J. Fluid Mech*. 235: 399–414, 1992.
22. **Gaver, D. P., and J. B. Grotberg.** The dynamics of a localized surfactant on a thin film. *J. Fluid Mech*. 213: 127–148, 1990.
23. **Gaver, D. P., D. Halpern, O. E. Jensen, and J. B. Grotberg.** The steady motion of a semi-infinite bubble through a flexible-walled channel. *J. Fluid Mech*. 319: 25–65, 1996.
24. **Gilliard, N., P. M. Richman, T. A. Merritt, and R. G. Spragg.** Effect of volume and dose on the pulmonary distribution of exogenous surfactant administered to normal rabbits or to rabbits with oleic acid lung injury. *Am. Rev. Respir. Dis*. 141: 743–747, 1990.
25. **Goldsmith, L. S., J. S. Greenspan, S. D. Rubenstein, M. R. Wolfson, and T. H. Shaffer.** Immediate improvement in lung volume after exogenous surfactant: alveolar recruitment vs. increased distention. *J. Pediatr*. 119: 424–428, 1991.
26. **Grotberg, J. B.** Pulmonary flow and transport phenomena. In: *Annual Review of Fluid Mechanics*, edited by J. L. Lumley, M. Van Dyke, and H. L. Reed. Palo Alto, CA: Annual Reviews, 1994, p. 529–571.
27. **Grotberg, J. B., and D. P. Gaver.** A synopsis of surfactant spreading research. *J. Colloid Interface Sci*. 178: 377–378, 1996.
28. **Grotberg, J. B., D. Halpern, and O. E. Jensen.** Interaction of exogenous and endogenous surfactant: spreading-rate effects. *J. Appl. Physiol*. 78: 750–756, 1995.
29. **Haefeli-Bleuer, B., and E. R. Weibel.** Morphometry of the human pulmonary acinus. *Anat. Rec*. 220: 401–414, 1988.
30. **Halpern, D., and D. P. Gaver.** Boundary element analysis of two-phase displacement in a Hele-Shaw cell. *J. Comp. Physiol. [A]* 115: 366–375, 1994.
31. **Halpern, D., and J. B. Grotberg.** Dynamics and transport of a localized soluble surfactant on a thin film. *J. Fluid Mech*. 237: 1–11, 1992.
32. **Halpern, D., and J. B. Grotberg.** Fluid-elastic instabilities of liquid-lined flexible tubes. *J. Fluid Mech*. 244: 615–632, 1992.
33. **Halpern, D., and J. B. Grotberg.** Surfactant effects on fluid-elastic instabilities of liquid-lined flexible tubes: a model of airway closure. *J. Biomech. Eng*. 115: 271–277, 1993.
34. **Hammond, P. S.** Nonlinear adjustment of a thin annular film of viscous fluid surrounding a thread of another within a circular pipe. *J. Fluid Mech*. 137: 363–384, 1983.
35. **Harris, J. D., F. Jackson, Jr., M. A. Moxley, and W. J. Longmore.** Effect of exogenous surfactant instillation on experimental acute lung injury. *J. Appl. Physiol*. 66: 1846–1851, 1989.
36. **Haslam, P. L., D. A. Hughes, P. D. MacNaughton, C. S. Baker, and T. W. Evans.** Surfactant replacement therapy in late-stage adult respiratory distress syndrome. *Lancet* 343: 1009–1011, 1994.
37. **Hazinski, T. A., P. A. Ladd, and C. A. DeMatteo.** Localization and induced expression of fusion genes in the rat lung. *Am. J. Respir. Cell Mol. Biol*. 4: 206–209, 1991.
38. **Heldt, G. P., T. A. Merritt, D. Golembeski, N. Gilliard, C. Bloor, and R. Spragg.** Distribution of surfactant, lung compliance, and aeration of preterm rabbit lungs after surfactant therapy and conventional and high-frequency oscillatory ventilation. *Pediatr. Res*. 31: 270–275, 1992.
39. **Holm, B. A., and S. Matalon.** Role of pulmonary surfactant in the development and treatment of adult respiratory distress syndrome. *Anesth. Analg*. 69: 805–818, 1989.
40. **Huppert, H. E.** Flow and instability of a viscous current down a slope. *Nature* 300: 427–429, 1982.
41. **Jensen, O. E.** The thin liquid lining of a weakly curved cylindrical tube. *J. Fluid Mech*. 331: 373–403, 1997.
42. **Jensen, O. E., and J. B. Grotberg.** Insoluble surfactant spreading on a thin viscous film: shock evolution and film rupture. *J. Fluid Mech*. 240: 259–288, 1992.
43. **Jensen, O. E., and J. B. Grotberg.** The spreading of heat or soluble surfactant on a thin liquid film. *Phys. Fluids A* 5: 58–68, 1993.

44. **Jensen, O. E., D. Halpern, and J. B. Grotberg.** Surfactant-driven flows on thin viscous films: pulmonary drug delivery. In: *Surface-Tension-Driven Flows*, edited by G. P. Neitzel and M. K. Smith. New York: Am. Soc. Mechanical Engineers, 1993, p. 47–55.
45. **Jensen, O. E., D. Halpern, and J. B. Grotberg.** Transport of a passive solute by surfactant-driven flows. *Chem. Eng. Sci*. 49: 1107–1117, 1994.
46. **Jobe, A. H.** Pulmonary surfactant therapy. *N. Engl. J. Med*. 328: 861–868, 1993.
47. **Kamm, R. D., and R. C. Schroter.** Is airway closure caused by a thin liquid instability? *Respir. Physiol*. 75: 141–156, 1989.
48. **Kendig, J. W., R. H. Notter, C. Cox, L. Reubens, J. M. Davis, W. M. Maniscalco, R. A. Sinkin, A. Bartoletti, H. S. Dweck, M. J. Horgan, H. Risemberg, D. L. Phelps, and D. Shapiro.** A comparison of surfactant as immediate prophylaxis and as rescue therapy in newborns of less than 30 weeks gestation. *N. Engl. J. Med*. 324: 865–871, 1991.
49. **Kharasch, V. S., T. D. Sweeney, J. Fredberg, J. Lehr, A. I. Damokosh, M. E. Avery, and J. D. Brain.** Pulmonary surfactant as a vehicle for intratracheal delivery of technetium sulfur colloid and Pentamidine in hamster lungs. *Am. Rev. Respir. Dis*. 144: 909–913, 1991.
50. **Leach, C. L., B. P. Fuhrman, F. C. Morin, and M. G. Rath.** Perfluorocarbon-associated gas exchange (partial liquid ventilation) in respiratory distress syndrome: a prospective, randomized, controlled study. *Crit. Care Med*. 21: 1270–1278, 1993.
51. **Lewis, J., M. Ikegami, R. Higuchi, A. Jobe, and D. Absolom.** Nebulized vs. instilled exogenous surfactant in an adult lung injury model. *J. Appl. Physiol*. 71: 1270–1276, 1991.
52. **Lewis, J. F., M. Ikegami, and A. H. Jobe.** Metabolism of exogenously administered surfactant in the acutely injured lungs of adult rabbits. *Am. Rev. Respir. Dis*. 145: 19–23, 1992.
53. **Lewis, J. F., and A. H. Jobe.** Surfactant and the adult respiratory distress syndrome. *Am. Rev. Respir. Dis*. 147: 218–233, 1993.
54. **Long, W., T. Thompson, H. Sundell, R. Schumacher, F. Volberg, and R. Guthrie.** Effects of two rescue doses of a synthetic surfactant on mortality rate and survival without bronchopulmonary dysplasia in 700- to 1350-gram infants with respiratory distress syndrome. The American Exosurf Neonatal Study Group I. *J. Pediatr*. 118: 595–605, 1991.
55. **Martinez, M. J., and K. S. Udell.** Boundary integral analysis of the creeping flow of long bubbles in capillaries. *J. Appl. Mech*. 56: 211–217, 1989.
56. **Matalon, S., B. A. Holm, and R. H. Notter.** Mitigation of pulmonary hyperoxic injury by administration of exogenous surfactant. *J. Appl. Physiol*. 62: 756–761, 1987.
57. **Moriarty, J., L. W. Schwartz, and E. O. Tuck.** Unsteady spreading of thin liquid films with small surface tension. *Phys. Fluids A* 3: 733–742, 1991.
58. **Novick, R. J., R. A. Veldhuizen, F. Possmayer, J. Lee, D. Sandler, and J. F. Lewis.** Exogenous surfactant therapy in thirty-eight hour lung graft preservation for transplantation. *J. Thorac. Cardiovasc. Surg*. 108: 259–268, 1994.
59. **Novotny, W. E., B. B. Hudak, S. Matalon, and B. A. Holm.** Hyperoxic lung injury reduces exogenous surfactant clearance in vivo. *Am. J. Respir. Crit. Care Med*. 151: 1843–1847, 1995.
60. **Pettenazzo, A., M. Ikegami, S. Seidner, and A. Jobe.** Clearance of surfactant phosphatidylcholine from adult rabbit lungs. *J. Appl. Physiol*. 64: 120–127, 1988.
61. **Pettenazzo, A., A. Jobe, J. Humme, S. Seidner, and M. Ikegami.** Clearance of surfactant phosphatidylcholine via the upper airways in rabbits. *J. Appl. Physiol*. 65: 2151–2155, 1988.
62. **Pettenazzo, A., K. Oguchi, S. Seidner, M. Ikegami, D. Berry, and A. Jobe.** Clearance of natural surfactant phosphatidylcholine from 3-day-old rabbit lungs: effects of dose and species. *Pediatr. Res*. 20: 1139–1142, 1986.
63. **Rider, E. D., M. Ikegami, and A. H. Jobe.** Intrapulmonary catabolism of surfactant-saturated phosphatidylcholine in rabbits. *J. Appl. Physiol*. 69: 1856–1862, 1990.
64. **Rider, E. D., M. Ikegami, and A. H. Jobe.** Localization of alveolar surfactant clearance in rabbit lung cells. *Am. J. Physiol*. 263 (*Lung Cell. Mol. Physiol*. 7): L201–L209, 1992.
65. **Rider, E. D., A. H. Jobe, M. Ikegami, and B. Sun.** Different ventilation strategies alter surfactant responses in preterm rabbits. *J. Appl. Physiol*. 73: 2089–2096, 1992.
66. **Schurch, S., H. Bachofen, J. Goerke, and F. Possmayer.** A captive bubble method reproduces the in situ behavior of lung surfactant monolayers. *J. Appl. Physiol*. 67: 2389–2396, 1989.
67. **Segerer, H., W. van Gelder, F. W. Angenent, L. J. van Woerkens, T. Curstedt, M. Obladen, and B. Lachmann.** Pulmonary distribution and efficacy of exogenous surfactant in lung-lavaged rabbits are influenced by the instillation technique. *Pediatr. Res*. 34: 490–494, 1993.
68. **Seidner, S. R., A. H. Jobe, L. Ruffini, M. Ikegami, and A. Pettenazzo.** Recovery of treatment doses of surfactants from the lungs and vascular compartments of mechanically ventilated premature rabbits. *Pediatr. Res*. 25: 423–428, 1989.
69. **Spragg, R. G., N. Gilliard, P. Richman, R. M. Smith, R. D. Hite, D. Pappert, B. Robertson, T. Curstedt, and D. Strayer.** Acute effects of a single dose of porcine surfactant on patients with the adult respiratory distress syndrome. *Chest* 105: 195–202, 1994.
70. **Taylor, G. I.** Deposition of a viscous fluid on the wall of a tube. *J. Fluid Mech*. 10: 161–165, 1961.
71. **Troian, S. M., E. Herbolzheimer, and S. A. P. R. L. Safran.** Model for the fingering instability of spreading surfactant drops. *Phys. Rev. Lett*. 65: 333–336, 1990.
72. **Tutuncu, A. S., K. Akpir, P. Mulder, W. Erdmann, and B. Lachmann.** Intratracheal perfluorocarbon administration as an aid in the ventilatory management of respiratory distress syndrome. *Anesthesiology* 79: 1083–1093, 1993.
73. **Ueda, T., M. Ikegami, E. D. Rider, and A. H. Jobe.** Distribution of surfactant and ventilation in surfactant-treated preterm lambs. *J. Appl. Physiol*. 76: 45–55, 1994.
74. **Weers, J. G.** A phyisicochemical evaluation of perfluorochemicals for oxygen transport applications. *J. Fluorine Chem*. 64: 73–93, 1993.
75. **Weibel, E. R.** *Morphometry of the Human Lung*. New York: Academic, 1963.
76. **Weibel, E. R., and D. M. Gomez.** Architecture of the human lung. *Science* 137: 577–585, 1962.
77. **West, B. J., V. Bhargava, and A. L. Goldberger.** Beyond the principle of similitude: renormalization in the bronchial tree. *J. Appl. Physiol*. 60: 1089–1097, 1986.
78. **Wiswell, T. E., S. S. Peabody, J. M. Davis, M. V. Slayter, R. C. Bent, and T. A. Merritt.** Surfactant therapy and high-frequency jet ventilation in the management of a piglet model of the meconium aspiration syndrome. *Pediatr. Res*. 36: 494–500, 1994.
79. **Wolfson, M. R., J. S. Greenspan, K. S. Deoras, S. D. Rubenstein, and T. H. Shaffer.** Comparison of gas and liquid ventilation: clinical, physiological, and histological correlates. *J. Appl. Physiol*. 72: 1024–1031, 1992.
80. **Wright, J. R.** Clearance and recycling of pulmonary surfactant. *Am. J. Physiol*. 259 (*Lung Cell. Mol. Physiol*. 3): L1–L12, 1990.
81. **Zelter, M., B. J. Escudier, J. M. Hoeffel, and J. F. Murray.** Effects of aerosolized artificial surfactant on repeated oleic acid injury in sheep. *Am. Rev. Respir. Dis*. 141: 1014–1019, 1990.